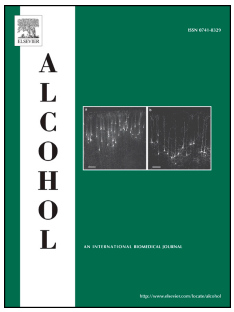


# Effect of Chronic Intermittent Ethanol Vapor Exposure on RNA Content of Brain-Derived Extracellular Vesicles

Annalisa M. Baratta, Regina A. Mangieri, Heather C. Aziz, Marcelo F. Lopez, Sean P. Farris, Gregg E. Homanics

PII: S0741-8329(22)00077-5

DOI: https://doi.org/10.1016/j.alcohol.2022.08.006

Reference: ALC 7155

To appear in: *Alcohol*

Received Date: 17 March 2022

Revised Date: 18 August 2022

Accepted Date: 18 August 2022

Please cite this article as: Baratta A.M., Mangieri R.A., Aziz H.C., Lopez M.F., Farris S.P. & Homanics G.E., Effect of Chronic Intermittent Ethanol Vapor Exposure on RNA Content of Brain-Derived Extracellular Vesicles, *Alcohol* (2022), doi: https://doi.org/10.1016/j.alcohol.2022.08.006.

# Effect of Chronic Intermittent Ethanol Vapor Exposure on RNA Content of Brain-Derived Extracellular Vesicles

Annalisa M. Baratta[a], Regina A. Mangieri[b], Heather C. Aziz[b], Marcelo F. Lopez[c], Sean P. Farris[a,d,e], and Gregg E. Homanics[a,d,f,g]*

[a] Center for Neuroscience, University of Pittsburgh School of Medicine, Pittsburgh, PA, USA
[b] College of Pharmacy, University of Texas at Austin, TX, USA
[c] Department of Psychiatry and Behavioral Science, Charleston Alcohol Research Center, Medical University of South Carolina, Charleston, SC, USA
[d] Department of Anesthesiology and Perioperative Medicine, University of Pittsburgh School of Medicine, Pittsburgh, PA, USA
[e] Department of Biomedical Informatics, University of Pittsburgh School of Medicine, Pittsburgh, PA, USA
[f] Department of Pharmacology and Chemical Biology, University of Pittsburgh School of Medicine, Pittsburgh, PA, USA
[g] Department of Neurobiology, University of Pittsburgh School of Medicine, Pittsburgh, PA, USA

***Correspondence:**
Gregg E. Homanics, Ph.D.
homanicsge@anes.upmc.edu

**Abstract:** Extracellular vesicles (EVs) are important players in normal biological function and disease pathogenesis. Of the many biomolecules packaged into EVs, coding and noncoding RNA transcripts are of particular interest for their ability to significantly alter cellular and molecular processes. Here we investigate how chronic ethanol exposure impacts EV RNA cargo and the functional outcomes of these changes. Following chronic intermittent ethanol (CIE) vapor exposure, EVs were isolated from male and female C57BL/6J mouse brain. Total RNA from EVs was analyzed by lncRNA/mRNA microarray to survey changes in RNA cargo following vapor exposure. Differential expression analysis of microarray data revealed a number of lncRNA and mRNA differentially expressed in CIE compared to control EVs. Weighted gene co-expression network analysis identified multiple male and female specific modules related to neuroinflammation, cell death, demyelination, and synapse organization. To functionally test these changes, whole cell voltage clamp recordings was used to assess synaptic transmission. Incubation of nucleus accumbens brain slices with EVs led to a reduction in spontaneous excitatory postsynaptic current amplitude, although no changes in synaptic transmission were observed between control and CIE EV administration. These results indicate that CIE vapor exposure significantly changes the RNA cargo of brain-derived EVs, which have the ability to impact neuronal function.

**Keywords:** Alcohol use disorder; extracellular vesicles; transcriptome; lncRNA; synaptic transmission

## Introduction

Alcohol use disorder (AUD) impacts millions of people each year, with ~95,000 individuals dying due to alcohol-related causes in the United States each year[1]. The hallmark symptoms of AUD are behavioral changes in which a person transitions from social to problem drinking despite negative consequences[2]. Additionally, a number of biological changes occur following chronic alcohol exposure, including transcriptomic, neuronal function, and neuroinflammatory alterations.

Extracellular vesicles (EVs) are small (30-1000nm), membrane-bound structures released by every cell-type. Originally believed to function in waste removal, recent research has highlighted the importance of EVs in normal biological processes. Purposefully packaged in the cell of origin, EVs are released into the extracellular space and mediate intercellular communication by binding to and releasing their cargo into a recipient cell[3,4]. EVs can contain a number of biomolecules, such as lipids[5,6], proteins[7,8], and nucleic acids[9–12], that have the ability to alter the molecular and biological processes of other cells. The term extracellular vesicle can encompass a number of vesicle subtypes, including exosomes (30-100nm) and microvesicles (100-1000nm)[13]. In the central nervous system (CNS), EVs support a number of functions including neuronal proliferation and differentiation, neurogenesis and circuit formation, and neuron-glia communication[14–17]. While required for normal function in the healthy brain, EV function can shift in response to disease or perturbation. They have been shown to perpetuate neuroinflammation[17–20] and contribute to CNS pathologies, such as Alzheimer's disease[21–24] and traumatic brain injury[25,26], underscoring their ability to negatively impact brain health.

The role of EVs in AUD, as well as how prolonged ethanol exposure impacts the biogenesis of EVs, has been largely understudied to this point. Outside of the CNS, studies have demonstrated that RNA and protein content of hepatocyte-derived EVs is altered following ethanol exposure and these changes induce inflammatory states in immune cells[27–31]. Within the CNS, the impact of ethanol exposure on the content and release of EVs from glial cells has been a primary focus. *In vitro* studies have demonstrated changes in the cargo of glial-derived EVs following ethanol exposure which induce inflammation in neighboring cells[18,32–35]. The EV cargo analysis of these studies focused on changes in protein content. While proteins control many of the major biological processes that directly impact the changes observed in AUD, they are not the only biomolecule found in EVs that could be controlling these effects.

Noncoding RNA (ncRNA) are increasingly being recognized as significant contributors to the control of normal biological functioning. As is evident by their name, ncRNA are transcribed portions of the genome that do not encode a protein. Of the many subtypes of ncRNA that have been identified, long noncoding RNA (lncRNA) are of particular interest for their ability to control multiple molecular and cellular processes. Generally defined as ncRNAs longer than 200 nucleotides in length and lacking an open reading frame[36], lncRNAs act as transcriptional activators or repressors, regulate alternative splicing, and impact protein expression[37–41]. LncRNA are one of the many biomolecules packaged into and transported by EVs, and there is evidence that their delivery into recipient cells can change biological processes[42,43]. As lncRNA have also been shown to impact ethanol-related behaviors[44,45], we investigated the intersection between EVs and lncRNA changes after ethanol exposure.

The present study aims to understand how chronic intermittent ethanol (CIE) vapor exposure impacts the RNA cargo of brain-derived EVs and investigate how these EVs impact neuronal function. Microarray analysis of total RNA isolated from brain-

derived EVs of both male and female animals following CIE revealed numerous differentially expressed lncRNAs and mRNAs involved in biological processes such as neuroinflammation and synapse organization. A male-specific change in genes related to glutamate receptor activity prompted us to functionally test male brain-derived EVs using whole cell voltage clamp recordings of medium spiny neurons (MSNs) in the nucleus accumbens (NAc); a brain-region known to be involved in the glutamatergic response to chronic ethanol exposure[46–48]. EV administration to brain slice preparations containing the NAc reduced spontaneous excitatory postsynaptic current (sEPSC) amplitude when compared to an EV-free control. However, no change was detected in any electrophysiological measure when comparing EVs isolated from CIE ethanol vs air control exposed animals. These results provide evidence that CIE induces changes in EV cargo with implications for neuronal function.

## Materials and Methods

### *Animals*

Adult (8 weeks at the start of exposure) male and female C57BL/6J were obtained from The Jackson Laboratory (Bar Harbor, ME). Tg(*Drd1a*-tdTomato)6Calak mice were bred at The University of Texas at Austin. All mice were housed in facilities fully accredited by the American Association for the Accreditation of Laboratory Animal Care. Mice were maintained on a 12/12h light-dark cycle and provided *ad libitum* access to food and water. Experiments were performed in accordance with the NIH Guide for the Care and Use of Laboratory Animals and were approved by the Institutional Animal Care and Use Committees at the Medical University of South Carolina, the University of Pittsburgh, and The University of Texas at Austin.

### *Chronic intermittent ethanol vapor exposure*

Two variations of the chronic intermittent ethanol (CIE) vapor exposure were performed, as previously described[49–52].

#### Treatment Group 1

In Pittsburgh, adult male and female C57BL/6J mice were exposed to ethanol vapor or room air conditions for 8h/day, 5 days/week, for four weeks (N = 10 per group per sex). Room air (8L/min) was passed through two heated Erlenmeyer flasks; one flask received ethanol (Decon Labs, King of Prussia, PA) via syringe pump (Harvard Apparatus, Holliston, MA). All animals remained group housed for the duration of the exposure. Temperature and humidity of each chamber was monitored daily and ranged between 23-25.5°C and 36-58% humidity. Ethanol levels in the vapor chamber were monitored by a custom sensor generously provided by Brian McCool (Wake Forest University). Following the fifth day of exposure each week, body weight was recorded and tail vein blood samples were collected using heparin-coated capillary tubes (Drummond, Broomall, PA) to determine blood ethanol concentrations (BECs). Plasma was analyzed on an Analox Alcohol Analyzer (AM1, Analox Instruments, Lunenburg, MA). Ethanol flow rate into the inhalation chamber was adjusted weekly based on BEC measurements the previous week to achieve BECs of 175-225 mg/dL. Immediately following the final ethanol exposure, mice were euthanized by $CO_2$ asphyxiation and whole brain was collected and stored at -80°C. EVs isolated from these brains (see below) were used for gene expression analysis.

Treatment Group 2

In Charleston, adult male C57BL/6J were also used. CIE mice were exposed to vapor exposure in inhalation chambers (16h/day, 4 days/week) while control mice were exposed to room air (N= 15 per group). CIE exposure was administered as previously described[53,54]. Mice were placed in Plexiglas inhalation chambers (60 x 36 x 60 cm) and exposed to ethanol vapor to achieve stable BECs in the range of 175-225 mg/dL. Before being placed in the chamber, ethanol intoxication was initiated by intraperitoneal (IP) administration of 1.6 g/kg ethanol (8% w/v; Warner Graham Co, Cockeysville, MD), and the alcohol dehydrogenase inhibitor pyrazole (1 mmol/kg i.p.; Sigma-Aldrich, St. Louis, MO) to stabilize blood ethanol levels. Control mice received pyrazole along with saline. Blood samples (40 µl) were collected from the retro-orbital sinus with heparinized capillary tubes during each cycle of exposure. Samples were centrifuged, and plasma was processed in an Analox Instrument analyzer (Lunenburg, MA). Four cycles of CIE exposure were completed over the course of four consecutive weeks with a 72h interval in between cycles. Mice were euthanized 24 hours after the last 16h exposure period on the fourth cycle. Brains were quickly collected and frozen. Samples were maintained at -80°C until they were shipped on dry ice to Pittsburgh. EVs isolated from these brains (see below) were used for electrophysiology.

*EV isolation and characterization*

EV isolation from brain tissue was achieved using differential ultracentrifugation as previously described[55]. Whole brains were separated into individual hemispheres and each hemisphere was processed separately. Using a razor blade, the tissue was finely minced with a few drops of 20 units/mL papain (Worthington Biochemicals, Lakewood NJ) in Hibernate A (Brain Bits LLC, Springfield, IL) warmed to 37°C. The tissue was then transferred into a 15 mL conical tube containing an additional 3.5 mL of papain in Hibernate A and allowed to incubate at 37°C for 20 minutes to achieve complete dissociation. Following incubation, 6.5 mL of ice cold Hibernate A with protease inhibitors (Sigma-Aldrich, St. Louis, MO; CAT# 04-693-159-001) was added to each tube and the solution was triturated with a serological pipette until the resulting mixture was homogenous. The samples then underwent two ten-minute centrifugations (300 x g and 2,000 x g), followed by a 30-minute centrifugation (10,000 x g) at 4°C, transferring the supernatant to a new tube each time and discarding the resulting pellet (Thermo Scientific Fiberlite F21-8x50y Rotor, k-factor 669.0). Following the third centrifugation, the supernatant was passed through a 0.2µm syringe filter and placed in 26.3 mL polycarbonate ultracentrifuge tubes (Beckman Coulter, Brea, CA). The remainder of the tube was filled with ice cold PBS. Tubes were centrifuged at 4°C and 100,000 x g for 70 minutes to pellet EVs (Beckman Coulter 70 Ti Fixed-Angle Rotor, k-factor 44). Following this first ultracentrifugation, the supernatant was discarded, the pellet resuspended in ice cold PBS, then the tube refilled with PBS and ultracentrifuged a second time. To collect the EVs following the final centrifugation, the supernatant was discarded and the pellet resuspended in 150µL of PBS before being placed in a 1.5 mL Eppendorf and stored at -80°C.

Electron microscopy (EM) and Nanoparticle Tracking Analysis (NTA) were used to characterize EVs. EM was performed in collaboration with the Center for Biologic Imaging at the University of Pittsburgh to observe the size and structure of isolated EVs. The specimens were mounted on formvar (Formvar15/19 resin, Electron Microscopy Sciences, Hatfield, PA) coated copper grids (200 mesh thick thin copper grids, Electron Microscopy Sciences, Hatfield, PA) and negative stained with 1% uranyl acetate (Uranyl

Acetate dihydrate, Electron Microscopy Sciences, Hatfield, PA) and on JEOL 1011 transmission electron microscope (JEOL) with a side mount AMT 2k digital camera (Advanced Microscopy Techniques, Woburn, MA). EV samples were sent to the Nanomedicines Characterization Core Facility at the University of North Carolina at Chapel Hill for NTA analysis. The particle concentration and size were determined using NanoSight 500 Version 3 (Malvern, USA). For the size measurements, EVs were diluted 1000-fold resulting in a final concentration of $1.3x10^9$ particles/mL in PBS. Five videos of 40 sec each were taken under the following exposure conditions (camera level 14). Unpaired Student's t-tests were used to analyze potential changes in EV size and concentration. Statistical analysis was performed in GraphPad Prism 8.0 (Graphpad Software Inc., San Diego, CA) and statistical significance was defined as $p < 0.05$.

*RNA isolation and microarray analysis*

To isolate RNA from EV samples, the SeraMir EV RNA Purification Kit (System Biosciences, Palo Alto, CA) was used according to manufacturer's instructions. Following RNA elution, purity, determined by the 260/280 ratio, and quantity was determined by Nanodrop spectrophotometer. Approximately 2.5µg of total RNA per sample (n = 6 samples per treatment per sex) were packaged on dry ice and shipped to Arraystar, Inc. (Rockville, MD). Purified RNA was amplified and transcribed into fluorescent cRNA and hybridized to the Mouse LncRNA Array v4.0 (8 x 60K, Arraystar). This array measures only lncRNA and mRNA. Arrays were scanned on an Agilent Scanner G2505C and images analyzed using Agilent Feature Extraction software (version 11.0.1.1). Quantile normalization was performed using the Bioconductor "preprocessCore" package in R. We chose to use microarrays in this study due to their ability to reliability quantify low expressing lncRNAs, as well as identify a number of lncRNA isoforms. Previous studies have attempted to optimize RNA-Seq to achieve similar detection, but reliable detection of a large number of lowly expressed lncRNA was not achievable[56].

*Differential expression and WGCNA*

Differential expression of reliably detected probes between control and CIE EV samples was performed using linear modeling (limma). So as not to eliminate any biologically relevant signal, analysis was performed on the full list of detected probes, rather than collapsing the data set into individual genes. To balance Type-I and Type-II error rates for downstream pathway analysis, statistical significance was set at an uncorrected p-value of 0.05. Next, we identified lists of genes that corresponded to the differentially expressed probe targets and entered them into Enrichr[57,58], an online tool used to identify common biological processes and molecular functions enriched in a set of genes. Due to the fact that male and female CIE vapor exposures were not performed concurrently, samples were analyzed separately.

The weighted gene co-expression network analysis (WGCNA) package in R[59] was used to identify co-expressing networks of genes, known as modules. WGCNA uses a dynamic tree-cutting algorithm based on hierarchical clustering of expression values to define modules (cutHeight = 0.99, minClusterSize = 400, softPower=18, type=signed). Differentially expressed modules ($p < 0.05$) between control and CIE samples were identified. As with differential expression analysis, Enrichr was used to determine common biological processes or molecular functions involving genes contained within each module.

*Bicinchoninic acid protein assay*

To determine surface protein concentration of EVs, the bicinchoninic acid (BCA) protein assay was performed. EV samples were diluted 1:5 in cold PBS to a final volume of 25µL in an Eppendorf tube. BCA assay reagent was made by mixing 9.8mL bicinchoninic acid (Sigma-Aldrich, St. Louis, MO) with 0.2mL $CuSO_4$ (Sigma-Aldrich, St. Louis, MO) and 500µL was added to each sample. Pre-prepared bovine serum albumin standards (0.0 – 2.0µg/mL) were included with each run. Standards and samples were incubated at 65°C for 30 minutes, followed by 10 minutes on ice. Finally, 200µL of each standard and sample was added to a 96-well plate, in duplicate, and the absorbance at 595nm was measured on a Tecan plate reader (Tecan, Männedorf, CH) (Control EVs: 237.67 $\pm$ 20.22 µg surface protein per sample; CIE EVs: 252 $\pm$ 41.92 µg surface protein per sample).

*Slice preparation*

Male Tg(*Drd1a*-tdTomato)6Calak mice[60] from an in-house managed colony at The University of Texas at Austin were used for electrophysiology experiments between 10-18 weeks of age. Tg(*Drd1a*-tdTomato)6Calak mice express the fluorescent protein tdTomato in dopamine D1 receptor-expressing (D1R+) cells. Thus, D1R+ cells can be visually identified via fluorescent excitation of tdTomato with 554 nm wavelength light. Isoflurane was used to lightly anesthetize mice before decapitation and brain removal. Brains were rapidly cooled in ice-cold artificial cerebral spinal fluid (ACSF) continuously bubbled with 95% $O_2$/5% $CO_2$ and composed of (in mM): 210 sucrose, 26.2 $NaHCO_3$, 1 $NaH_2PO_4$, 2.5 KCl, 11 glucose, 6 $MgSO_4$, and 2.5 $CaCl_2$. A VT-1000S vibratome (Leica, Wetzlar, DE) was used to make 240 µM thick sagittal slices containing the NAc shell. At the time of slice preparation, frozen samples (300 µL PBS ± EVs from air- or CIE-treated male mice; 187µg per sample) were defrosted and added to one of three low-volume brain slice keepers (Automate Scientific) that contained 5.5 mL of aCSF composed of (in mM): 124 NaCl, 26 $NaHCO_3$, 10 dextrose, 4.4 KCl, 1 $NaH_2PO_4$, 2.4 $MgSO_4$, and 1.8 $CaCl_2$. This recovery solution was constantly bubbled with 95% $O_2$/5% $CO_2$ and maintained at 32°C. Immediately after cutting, slices were placed in the recovery aCSF (one slice per recovery chamber containing 187µg EVs in a total volume of 5.8 mL). Slices were incubated for a minimum of 6 h before transferring to the recording bath. The average time from slice preparation to recording acquisition (time in vitro, incubation time plus time in the recording chamber) was 8.9 h, with a range of 6.6 - 11.5 h. Incubation time periods shorter than 6 hours were not tested, as we hypothesized the effects of exosomes would not be immediate but would be mediated via RNA-induced changes in gene expression and protein synthesis. Pilot studies testing longer incubation time points indicated 14-24 hours was sufficient to observe exosome-induced changes in excitatory synaptic transmission. However, we could not consistently obtain viable whole-cell recordings in acute brain slices from adult mice after 14-24 hours in vitro, leading to the testing of a shorter incubation window.

*Electrophysiology data acquisition and acquisition*

Recordings were performed in ACSF composed of (in mM): 124 NaCl, 26 $NaHCO_3$, 10 dextrose, 4.4 KCl, 1 $NaH_2PO_3$, 1.2 $MgSO_4$, and 2.0 $CaCl_2$, pumped into the chamber at a rate of ~2 mL/min and maintained at 32-33°C. Whole-cell recordings were

made using electrodes with resistances ranging from 4-7 MΩ, produced from 4" thin-walled glass capillaries (1.5OD/1.12ID, World Precision Instruments, Sarasota, FL) using a P-97 Flaming/brown micropipette puller (Sutter Instruments, Novato, CA). Recording electrodes were filled with an intracellular solution composed of (in mM): 120 $CsMeSO_3$, 5 NaCl, 10 HEPES, 10 TEA-Cl, 1.1 EGTA, 4 $Mg^{2+}$-ATP, 0.3 Na-GTP and 1 mg/mL QX-314-Br[61]. All electrophysiology reagents were obtained from Sigma-Aldrich or Fisher Scientific, unless otherwise noted.

Whole-cell recordings were collected in the medial shell of the NAc. We targeted dopamine D1 receptor-expressing (D1R+) medium spiny neurons for recordings because prior work has specifically implicated these neurons as being regulated by CIE exposure[62,63]. Neurons were visually identified as D1R+ by the presence of epifluorescence using an MRK200 Modular Imaging system (Siskiyou Corporation, Grants Pass, OR) mounted on a vibration isolation table. Data were acquired on two electrophysiology recording stations: one utilizing a CV203BU headstage and Axopatch 200B amplifier, the other utilizing a CV-7B headstage and MultiClamp 700B amplifier software, with filtering at 2 kHz, and digitization at 5 or 10 KHz through Digidata 1440A interface boards using Clampex 10.3 or 10.7 (all products by Molecular Devices, San Jose, CA). After obtaining whole-cell access, the intracellular solution was allowed 10 minutes to dialyze. We used recording conditions that allowed for measurement of both excitatory and inhibitory synaptic transmission in the same neuron[61,64]. Cells were voltage clamped at -55 mV and sEPSCs were recorded for 3 minutes, after which cells were held at +10 mV and sIPSCs were recorded for 3 minutes. Any experiment during which access resistance (Ra) changed by more than 20% or exceeded 31 MΩ was excluded from statistical analysis. Average spontaneous postsynaptic current frequency, and distributions of event amplitudes and inter-event intervals were determined using a 2-3 minute analysis window. Clampfit 10.7 Template Search was used to identify excitatory and inhibitory currents and events were manually inspected and verified. sEPSC and sIPSC events for kinetics analyses (10%-90% of peak rise time, 90%-10% of peak decay time, and peak area) were identified using the Template Search feature (Clampfit 11.0) and only non-overlapping events were manually accepted for analysis. For sEPSCs, a minimum of 66 events (140 events on average) per neuron were used for kinetics analyses. For sIPSCs, only neurons having at least 40 events available for analysis were included in the kinetics data sets; on average, 80 events per neuron used for kinetics analyses. Excitatory drive (sEPSC frequency x sEPSC amplitude) and inhibitory drive (sIPSC frequency x sIPSC amplitude) were calculated for each cell and synaptic drive was defined as excitatory drive divided by inhibitory drive.

Statistical analysis of electrophysiology data was performed in GraphPad Prism 8.0-9.3. Statistical significance was defined as $P < 0.05$. Cumulative probability distributions of binned data were analyzed using two-way mixed ANOVA (with treatment group as the between-groups factor and bin as the within-subjects factor). One-way ANOVA, unpaired Student's t-tests or Welch's t-tests (for groups with unequal variances) were used to compare group differences in the mean values of electrophysiological measures. Datasets for the room-air ("Air") and ethanol ("CIE") EV groups were either treated as independent datasets or were compared to PBS as a pooled dataset for EVs overall ("EVs"), according to the following rationale. Cumulative probability distributions of Air and CIE data were first compared to each other; when

distributions were not significantly different (i.e., there was no main effect of group or bin x group interaction), data from these two groups were pooled and EVs overall were compared to the PBS control treatment group. When Air and CIE distributions were significantly different from each other, these two groups were treated as independent datasets and comparisons were made across all three treatment groups (ANOVAs performed with three levels of group). Significant group or bin x group interaction effects in ANOVAs with three levels of group were followed up with Tukey's multiple comparisons and, as appropriate, additional, separate two-way ANOVAs with two levels of group (to compare distributions of PBS versus Air and PBS versus CIE). Non-linear regression was used to analyze normalized frequency (events per bin/total number of events) histograms of binned electrophysiology data, and regression curve fits were compared using the Extra Sum-of-Squares F-test.

## Results

*Brain-derived EV characterization following chronic intermittent ethanol vapor exposure*

To characterize EV samples isolated by differential ultracentrifugation from treatment group 1, NTA and EM were performed. NTA displayed a significant enrichment for vesicles under 200nM in size **(Figure 1A)**. EM images of the samples confirmed the size of vesicles within the sample, as well as revealed the characteristic cup shape generally associated with EVs[65,66] **(Figure 1B)**. NTA revealed no significant change in the size or concentration of brain-derived EVs following CIE vapor exposure compared to control exposure in our preparations **(Figure 1C, D)** (Control EVs: 5.96e17 ± 1.12e17 particles per undiluted preparation; CIE EVs: 5.77e17 ± 6.35e16 particles per undiluted preparation). EVs isolated from treatment group 2 were characterized using NTA and no change in size or concentration within our sample preparations was observed **(Supplementary Figure 1)**.

*LncRNA/mRNA microarray differential expression analysis*

To maintain a consistent background between male and female samples, lists of detected probes were overlapped and pared down to include only probes detected in both datasets. This left a total of 39,125 probes reliably detected in male and female samples corresponding to 25,865 currently recognized genes (11,752 lncRNA and 14,113 mRNA). Analysis of total RNA isolated from female brain-derived EVs revealed 3181 differentially expressed probe targets (DEPTs). We observed a greater incidence of upregulated DEPTs (2,141 upregulated and 1,040 downregulated), as well as more changes in lncRNA (1,972) than mRNA (1,209), when comparing control and CIE female EVs **(Figure 2A,B)**. The top ten DEPTs consisted of six lncRNAs, four of which are unannotated, and four protein coding genes **(Table 1)**. All ten of these DEPTs were upregulated. An unannotated lncRNA, AK155383, was the top DEPT and significantly upregulated in female EVs (FC = 2.40; $P < 0.001$). Results for differential expression analysis for all detected probes are included in **Supplementary Table 1.**

Enrichr was used to identify biological processes associated with significantly upregulated genes. Gene ontology analysis revealed changes in immune related processes such as 'regulation of type I interferon production' (GO: 0032479, P = 0.0030), supporting a possible role for EVs as immune modulators following ethanol exposure **(Table 2)**. Full results for Enrichr analysis are provided in **Supplementary Table 2.**

Analysis of total RNA from male brain-derived EVs indicated a much lower incidence of DEPTs, with only 1003 achieving statistical significance. As observed in the female samples, greater changes occurred in DEPTs representing lncRNAs (666 lncRNAs and 337 mRNAs), although there was a general downregulation in expression when comparing control and CIE male EVs (449 upregulated and 554 downregulated) **(Figure 2C,D)**. LncRNAs were vastly overrepresented in the top ten DEPTs, with eight identified as lncRNAs, of which 5 are unannotated **(Table 3)**. The top DEPT corresponded to a noncoding transcript of Bromodomain Containing 8 (*Brd8*), which was significantly upregulated in CIE EVs (FC = 2.05; P < 0.001). Results for differential expression analysis for all detected probes are included in **Supplementary Table 3.**

Gene ontology analysis for statistically significant downregulated genes revealed changes in 'fibroblast growth factor-activated receptor activity' (GO: 0005007, P = 0.0011). Fibroblast growth factor receptor 1 (*Fgfr1*), which codes for a protein involved in survival of nerve cells and inhibition of which suppresses alcohol consumption[67], was significantly downregulated in CIE EVs (P = 0.0422). Additionally, changes related to 'glutamate receptor activity' (GO: 0008066, P = 0.0171), which is a known consequence of acute and chronic alcohol exposure, were observed **(Table 4**). Full results for Enrichr analysis are provided in **Supplementary Table 4.** This male specific change in glutamate receptor functioning prompted us to functionally test these results in later experiments (see below). It is interesting to note that there was very little overlap in DEPTs between male and female EVs (**Figure 3**), 102 probes of which 39 were changed in opposite directions (**Supplementary Table 5**), indicating that RNA cargo of EVs following chronic ethanol exposure may control sexually-distinct biological processes in the brain.

*Gene co-expression networks*

Weighted gene co-expression network analysis (WGCNA) was performed to identify coordinately regulated clusters of biological transcripts, known as modules, in brain-derived EV samples. Analysis of female samples revealed 21 distinct modules (abbreviated FM vs those from males which are abbreviated MM). Fourteen FMs were differentially expressed between control and CIE samples, nine of which were up-regulated **(Table 5)**. The size of modules ranged from 519 to 12,547 probe targets. Analysis of male samples generated 35 different modules of which eleven were differentially expressed **(Table 6)**. MM sizes ranged from 430 to 2778 probe targets. Gene ontology analysis was performed on all modules to identify biological processes and molecular functions controlled by these coordinated sets of genes. As with the differential expression analysis, a number of modules with unique gene annotations were observed between male and female samples.

Although 14 FMs were differentially expressed, FM_8 stands out as being the only module in either male or female samples related to apoptosis. FM_8 was significantly down-regulated in CIE EVs (P = 0.0456). Gene ontology analysis of the module revealed genes involved in 'negative regulation of intrinsic apoptotic signaling pathway' (GO: 2001234, P = 0.0010), 'negative regulation of release of cytochrome c from mitochondria (GO: 0090201, P = 0.0057), and 'negative regulation of neuron death' (GO: 1901215, P = 0.0378). Cytochrome c-induced activation of caspases and apoptosis, in the periphery and brain, are known consequences of ethanol exposure[68–70]. Of the genes included in this module, expression and activity of AKT serine/threonine kinase 1 (*Akt1*), secretogranin 2 (*Scg2*), and matrix metalloproteinse-9 (*Mmp9*) are upregulated in response to ethanol[71–73]. Additionally, overexpression of *Mmp9*

decreases ethanol consumption and preference in mice[74]. When surveying male modules, gene ontology analysis related to apoptosis was not observed, highlighting this as a possible female specific mechanism.

Of the 11 differentially expressed male-specific modules identified by WGCNA, MM_5 was significantly down-regulated in CIE EVs (P = 5.75e-21) and unique among all male and female modules in its function. Analysis with Enrichr indicated that genes in this module are responsible for 'myelination in the peripheral nervous system' (GO: 0022011, P = 0.0028), 'peripheral nervous system axon ensheathment (GO: 0032292, P = 0.0042), and 'Schwann cell development' (GO: 0014044, P = 0.0042). As many of the genes included in these biological processes are also expressed in the CNS, this implies that disruptions in myelin integrity are not limited to the periphery. This finding is not surprising, as acute and chronic ethanol exposure can lead to myelin damage and demyelination in both rodent and human studies[75–78]. Two genes identified as part of this module, neurofibromin 1 (*Nf1*) and myelin transcription factor 1 (*MyT1*), are expressed in oligodendrocytes and Schwann cells and play a role in promoting myelination[79–81]. Altering expression of either gene significantly changes a number of ethanol-related behaviors[82,83]. The male-specific biological function of this module indicates that male animals may be more susceptible to the demyelinating effects of chronic ethanol compared to female animals[77].

Despite the differences discussed above, a number of modules in male and female EVs with overlapping biological functions were identified. Increases in neuroinflammation are regularly observed following ethanol exposure, so the appearance of modules in both sexes related to this is expected. Gene ontology analysis of FM_18 identified a number of biological processes, including 'regulation of toll-like receptor signaling pathway' (GO: 0034121, P = 0.0135), 'regulation of interleukin-6 production' (GO: 0032675, P = 0.0147), 'regulation of tumor necrosis factor production' (GO: 0032680), and 'regulation of interferon-gamma-mediated signaling pathway' (GO: P = 0.0444, down). In MM_19, biological processes related to 'positive regulation of toll-like receptor 9 signaling pathway' (GO: 0034165, P = 0.0165) and 'positive regulation of toll-like receptor 7 signaling pathway' (GO: 0034157, P = 0.0241) were observed. Both FM_18 (P = 2.96e-13) and MM_19 (P = 3.10e-121) were significantly differentially expressed in CIE EVs, but in different directions. FM_18 was up-regulated while MM_19 was downregulated. This indicates that there may be broad similarities in the immune response to ethanol, such as toll-like receptor signaling and cytokine production, but the mechanism by which EVs impact these differs between the sexes.

Another biological process that appears in multiple modules across both male and female samples is dendrite formation and synapse assembly. Genes in these modules regulate 'positive regulation of dendritic spine development (GO: 0060999, MM_31, P = 0.0017), 'synapse assembly' (GO: 0007416, MM_13, P = 0.0253), 'regulation of dendrite morphogenesis' (GO: 0048814, FM_3, P = 0.0099), and 'presynaptic active zone organization' (GO: 1990709, FM_3, P = 0.0147). More specifically, biological processes related to 'glutamate receptor signaling pathway' (GO: 0007215, P = 0.0203) and 'glutamate receptor activity' (GO: 0008066, P = 0.0171) were observed only in male modules, mirroring our findings in the gene ontology analysis of DEPTs in male EVs. As this alteration in genes related to glutamate receptor activity was male specific, we functionally tested the outcome of EVs on synaptic transmission using only male brain-derived EVs. Full results of WGCNA and Enrichr analysis are included in **Supplementary Tables 6 (female) and 7 (male).**

*Effects of EVs on synaptic transmission*

To functionally test coordinated changes in gene expression within EVs due to CIE, we examined the effects of male control (Air) and CIE EVs on synaptic transmission. We hypothesized that coordinated changes in genes related to glutamate receptors activity, observed only in male animals, would alter synaptic properties within the NAc, a brain region involved in the rewarding aspects of ethanol (83–85). Acute brain slices were prepared from adult male mice; immediately after cutting, slices were placed in a recovery bath containing aCSF, to which EVs (previously isolated from the brains of CIE-treated or Air-treated male mice), or a vehicle-control solution (PBS) had been added. Slices were incubated for a minimum of 6 h before transfer to the recording chamber. sEPSCs were observed at a membrane holding potential of -55 mV (**Figure 4A**), and spontaneous inhibitory postsynaptic currents (sIPSCs) were observed at +10 mV (**Figure 4H**). Current traces were analyzed to determine the amplitude and frequency of spontaneous excitatory and inhibitory events, as well as measures of event kinetics. For each electrophysiological measure, we first compared the cumulative probability distribution of the CIE-EV treatment group (CIE group) to that of the Air-EV treatment group (Air group). If the CIE and Air group distributions significantly differed from each other, these two groups were treated as independent datasets and comparisons were made across all three treatment conditions. For measures in which there were no significant differences between the CIE and Air group distributions, we collapsed these groups and used the pooled dataset to analyze whether EVs overall were different from the PBS control group.

For sEPSC amplitude, analyses of the cumulative probability distributions revealed a significant bin x group interaction ($F_{22,462} = 2.15$, $P = 0.0017$) when comparing CIE to Air, and we therefore performed two-way ANOVA with all three groups, which revealed both a main effect of group ($F_{2,33} = 3.32$, $P = 0.049$) and bin x group interaction ($F_{44,726} = 2.63$, $P < 0.0001$, **Figure 4B**). Further investigation of this interaction revealed that, compared to PBS, the CIE cumulative probability distribution was left-shifted (main effect of group, $F_{1,22} = 6.38$, $P = 0.019$, bin x group interaction, $F_{22,484} = 5.71$, $P < 0.0001$) and the mean sEPSC amplitude (**Figure 4C**) was reduced (main effect of group in one-way ANOVA, $F_{2,33} = 3.34$, $P = 0.048$, Tukey's multiple comparisons test, $q_{33} = 3.64$, $P = 0.038$). In contrast, there were no significant differences between Air and PBS cumulative distributions (no main effect of group, $F_{1,23} = 1.51$, $P = 0.23$, or bin x group interaction, $F_{22,506} = 0.71$, $P = 0.83$) or mean sEPSC amplitudes (Tukey's multiple comparisons test, $q_{33} = 1.95$, $P = 0.36$). sEPSC area (charge transfer) distributions (**Figure 4D** inset) did not differ between Air and CIE (no main effect of group, $F_{1,21} = 0.59$, $P = 0.45$, or bin x group interaction, $F_{17,357} = 0.36$, $P = 0.99$). However, the cumulative probability distribution of the pooled EV data was left-shifted relative to PBS (main effect of group, $F_{1,34} = 6.12$, $P = 0.019$, bin x group interaction, $F_{11,374} = 3.19$, $P = 0.0004$, **Figure 4D**) and the mean sEPSC area was reduced by EVs (unpaired t-test, $t_{34} = 2.243$, $P = 0.021$, **Figure 4E**). sEPSC rise times (10%-90%) did not significantly differ between Air and CIE groups (no main effect of group, $F_{1,21} = 1.49$, $P = 0.24$, or bin x group interaction, $F_{16,336} = 1.38$, $P = 0.15$, **Supplementary Figure 2A inset**) and were not affected by EVs overall (no main effect of group, $F_{1,34} = 0.11$, $P = 0.74$, or bin x group interaction, $F_{16,544} = 0.32$, $P = 0.995$, **Supplementary Figure 2A, B**). There was a statistically significant bin x group

interaction when comparing decay time (90-10%) distributions between Air and CIE groups ($F_{25,525}$ = 1.60, P = 0.033, **Figure 4F**). However, two-way ANOVA of all three group distributions did not indicate a statistically significant effect of group ($F_{2,33}$ = 1.57, P = 0.22) or bin x group interaction ($F_{50,825}$ = 1.22, P = 0.15) and mean decay time did not differ between all three groups (one-way ANOVA, $F_{2,33}$ = 1.63, P = 0.21, **Figure 4G**). The distributions of inter-event intervals did not differ between Air and CIE groups (no main effect of group, $F_{1,21}$ = 0.41, P = 0.53 or bin x group interaction, $F_{57,1197}$ = 0.2, P > 0.9999, **Supplementary Figure 2C inset**). EVs overall altered the cumulative distribution of inter-event intervals (bin x group interaction, $F_{57,1938}$ = 1.59, P = 0.0035, **Supplementary Figure 2C**), but the mean sEPSC frequency for EVs was not significantly greater than that of PBS (unpaired t-test, $t_{34}$ = 1.26, P = 0.21, **Supplementary Figure 2D**).

In regard to inhibitory synaptic transmission, the distributions of sIPSC amplitudes did not differ between CIE and Air groups (no effect of group, $F_{1,21}$ = 0.32, P = 0.58, or bin x group interaction, $F_{22,462}$ = 0.81, P = 0.72, **Supplementary Figure 2E inset**). There was a significant bin x group interaction when comparing EVs overall to PBS ($F_{22,748}$ = 1.99, P = 0.005, **Supplementary Figure 2E**), but mean sIPSC amplitudes were not different (unpaired t-test of EVs versus PBS, $t_{34}$ = 0.11, P = 0.91, **Supplementary Figure 4F**). sIPSC area (charge transfer) distributions did not differ between CIE and Air groups (no main effect of group, $F_{1,18}$ = 1.12, P = 0.30, or bin x group interaction, $F_{33,594}$ = 0.43, P = 0.99, **Supplementary Figure 2G inset**). EVs overall did not did not change the cumulative probability distribution relative to PBS (no main effect of group, $F_{1,28}$ = 0.12, P = 0.73, or bin x group interaction, $F_{33,924}$ = 1.44, P = 0.052, **Supplementary Figure 2G**), and there was no difference in the average sIPSC charge transfer between EVs and PBS (unpaired t-test, $t_{28}$ = 0.43, P = 0.67, **Supplementary Figure 2H**). CIE and Air groups did not differ from each other in regard to sIPSC rise time (10%-90%) distributions (no main effect of group, $F_{1,18}$ = 0.52, P = 0.48, or bin x group interaction, $F_{30,540}$ = 1.10, P = 0.33, **Figure 4I inset**). EVs overall, however, showed a right-shift in the cumulative probability distribution (main effect of group, $F_{1,28}$ = 4.71, P = 0.039, bin x group interaction, $F_{30,40}$ = 4.40, P < 0.0001, **Figure 4I**) and increase in the mean rise time relative to PBS (unpaired t-test, $t_{28}$ = 2.20, P = 0.036, **Figure 4J**). The cumulative distributions of sIPSC decay times (90-10%) were significantly different between Air and CIE groups (bin x group interaction, $F_{30,540}$ = 3.07, P < 0.0001) and two-way ANOVA of all three groups also revealed a significant bin x group interaction ($F_{60,810}$ = 2.76, P < 0.0001, **Figure 4K**). Further investigation of this interaction revealed that the CIE cumulative probability distribution was also significantly different from PBS (main effect of group, $F_{1,18}$ = 5.28, P = 0.034, bin x group interaction, $F_{30,540}$ = 4.59, P < 0.0001), while Air was not different from PBS (no main effect of group, $F_{1,18}$ = 0.26, P = 0.62, or bin x group interaction, $F_{30,540}$ = 0.27, P > 0.9999). All three groups exhibited sIPSC event populations that were comprised of faster (~15 ms on average)- and slower (>25 ms)-decaying events (**Figure 4L**). However, analysis of normalized frequency histograms revealed that the Air group distribution was better fit by a single Gaussian than a sum of two Gaussians (Extra Sum-of-Squares F-test, $F_{3,19}$ = 2.29, P = 0.11), while the CIE group distribution was better fit as a sum of two Gaussians (Extra Sum-of-Squares F-test, $F_{3,19}$ = 43.64, P < 0.0001), as was PBS (Extra Sum-of-Squares F-test, $F_{3,19}$ = 8.68, P = 0.0008). The best-fit (sum of two Gaussians)

curves for the CIE and PBS distributions were significantly different from each other (Extra Sum-of-Squares F-test, $F_{6,38} = 7.51$, $P < 0.0001$). Thus, CIE EVs in particular increased the relative frequency of slow-decaying sIPSC events. Although this effect of CIE EVs did tend to increase the mean sIPSC decay time, group differences in mean decay time (**Figure 4M**) were not at the level of statistical significance (1-way ANOVA, $F_{2,27} = 2.90$, $P = 0.07$). The cumulative probability distributions of sIPSC inter-event intervals did not differ between Air and CIE groups (no main effect of group, $F_{1,21} = 0.0002$, $P = 0.98$ or bin x group interaction, $F_{32,672} = 0.08$, $P > 0.9999$, **Supplementary Figure 2I inset**). EVs overall did not alter the cumulative distribution of inter-event intervals (no main effect of group, $F_{1,34} = 0.22$, $P = 0.65$ or bin x group interaction, $F_{32,1088} = 0.16$, $P > 0.9999$, **Supplementary Figure 2I**), and the mean sIPSC frequency for EVs overall was not significantly different than that of PBS (unpaired t-test, $t_{34} = 0.52$, $P = 0.61$, **Supplementary Figure 2J**).

Finally, we calculated a measure of net synaptic drive (amplitude x frequency of sEPSCs divided by amplitude x frequency of sIPSCs) for each recorded neuron (**Supplementary Figure 2K**). There was no difference in synaptic drive between CIE and Air groups (unpaired t-test, $t_{21} = 0.36$, $P = 0.72$) or EVs overall compared to PBS (Welch-corrected unpaired t-test, $t_{14.08} = 0.67$, $P = 0.51$).

## 4. Discussion

The primary aim of the current study was to determine how CIE vapor exposure impacted the RNA content of whole brain-derived EVs. We saw an array of changes in mRNA and lncRNA expression within EVs which, when analyzed by WGCNA and gene ontology, revealed changes in genes related to myelination, apoptosis, neuroinflammation, and synapse organization. Male specific changes in genes associated with glutamate receptor activity prompted us to functionally test the impact of these EVs on neuronal function using electrophysiology. We determined that EV application compared to PBS control exposure reduced sEPSC amplitude. Although no changes in synaptic activity were observed when comparing control EV vs CIE vapor EV exposure, we did observe time-related changes in synaptic transmission that differed between the two EV groups.

Our findings that brain-derived EVs in general contain RNAs associated with processes such as neuroinflammation, myelination, and apoptosis are consistent with the current literature. BV2 microglia and primary astrocyte EVs both show increases in proinflammatory related proteins following ethanol exposure which can compromise neuronal survival when added to neuronal cultures[32,33]. Experiments in organotypic brain slice cultures have yielded similar results, with application of EVs from ethanol exposed cultures inducing neuroinflammation in naïve cultures[18]. Most studies exploring the role of EVs in myelin damage have focused on demyelinating disorders. While increases in neuroinflammation are thought to produce one of the greatest insults to myelin[84], EVs also contain many myelin associated proteins, such as myelin basic protein and myelin oligodendrocyte glycoprotein[85–88], whose changes in expression may compromise myelin integrity[89]. Finally, the ability of EVs to induce apoptosis has been primarily observed in the periphery. Studies have shown that peripherally released EVs induce apoptosis through activation of both mitogen-activated protein kinase (MAPK) and oxidative stress pathways[90,91]. However, Lin et al., (2021) demonstrated that brain-derived EVs can enter the blood stream and induce apoptosis in peripheral cells[92],

suggesting that EVs from the CNS also possess the machinery to negatively impact cell survival.

While the phenomena of neuroinflammation, myelin damage, and cell death have all been studied in the context of AUD, and we identified significantly differentially expressed modules related to each of these processes, it is unlikely that they are acting independently. Changes in any one of these pathways can set off a cascade, negatively impacting the rest. For instance, the release of proinflammatory cytokines such as TNF-α and IFN-γ induces apoptosis pathways, leading to cell death[93–96]. Oligodendrocytes are one of the many cell types affected by this cascade[93,97], and their death results in myelin damage and demyelination[98,99]. Additionally, activation of immune pathways can independently induce myelin damage[100] and impact synaptic function[101]. Ultimately, demyelination will compromise the ability of neurons to function and negatively impact cellular communication and synaptic transmission[102,103]. Our data suggests that EVs play in role in either inducing or perpetuating these damaging effects of ethanol, but future studies are needed to unravel exactly how intercellular communication by EVs controls these processes.

Acute and chronic ethanol treatment have been shown to elicit changes in glutamatergic and GABAergic synaptic transmission in the NAc[104]. Here, we used a technique that allowed us to assess both forms of transmission in the same neuron, and in summary, our findings indicated that EVs differentially impacted both excitatory and inhibitory events. EV treatment affected sEPSC, but not sIPSC, amplitude and charge transfer. CIE EVs, in particular, increased the probability of smaller amplitude sEPSC events and reduced the average sEPSC amplitude, and EV treatment overall decreased the average sEPSC charge transfer, relative to the PBS control treatment group. sEPSC rise times were completely unaffected by EV treatment, and although the cumulative probability distributions suggested that CIE EVs tended to prolong sEPSC decay times relative to Air EVs, there was no statistically significant main effect across all three treatment groups. In contrast, EVs overall prolonged sIPSC rise times, and the distribution of sIPSC decay times was specifically altered in the CIE EV treatment group, which had an increased probability of slower-decaying events. There were no statistically significant group differences in the average event frequency for either sEPSCs or sIPSCs, or in excitatory/inhibitory balance (synaptic drive). All together, these findings indicate that EVs influence synaptic transmission in the NAc, and may do so by regulating receptor trafficking and subunit composition at synapses.

The electrophysiology results are limited in several important ways. As part of these experiments, we did not independently verify that EVs were taken up by the D1 MSNs. Despite this, we are confident that these cells were able to effectively internalize the EVs, as multiple previous studies have demonstrated this phenomenon[15,105,106]. Also, EVs may alter synaptic transmission on time scales that are outside the range in which data was collected. Recent work by Vilcaes et al. (2021) has shown that GABA release (IPSC frequency) in hippocampal neuron cultures can be augmented within 30-60 minutes of application of neuronally-derived EVs[107]. This study showed that these EVs contain synaptic vesicle-associated proteins, such as synaptobrevin, which integrate into the presynaptic membrane and promote GABA release. Thus, proteinaceous components of EVs could have altered synaptic activity prior to the window of time in which our experiments were conducted. At present, the mechanisms underlying our electrophysiology findings are unclear. The divergent effects on excitatory versus inhibitory event amplitudes and kinetics, and effects by CIE EVs in

particular, argues against the possibility that EVs generally disrupted channel function through non-specific physical interactions. One possibility is that EVs exert control of gene expression that leads to changes in synaptic transmission. Peng et al. (2021) report that neuronally-derived EVs can alter expression of cytokines, such as interleukin-10[35]. Interleukin-10, in turn, can regulate both GABA receptor kinetics [108,109] and AMPA glutamate receptor trafficking[110]. This suggests the intriguing hypothesis that the observed effects of EV treatment on sEPSCs and sIPSCs could both be mediated by EV-elicited regulation of cytokine expression and signaling. Our approach was also limited in that we focused our investigation on NAcSh D1 MSNs. We focused on NAcSh D1 MSNs because of our prior work showing that glutamate synapses in this neuronal subtype, in this NAc subregion in particular, are altered by chronic ethanol treatment[62,63]. However, D2 MSNs are another major output pathway from the NAc and future studies are necessary to understand whether EVs can influence synaptic excitation or inhibition of these neurons. Finally, the downstream consequences of EV-mediated regulation of NAc D1 MSN synapses are unclear. In MSNs, the relationship between synaptic input and the intrinsic excitability, or overall output of the neuron, is not straightforward, as MSNs can adjust their level of membrane excitability to compensate for changes in synaptic input[111].

While the primary focus of this research was the lncRNA content of EVs, many other biomolecules may be altered following ethanol exposure. Evidence of microRNA (miRNA) and circular RNA (circRNA) in EVs has been noted and these noncoding RNA subtypes have the ability to alter cellular processes[112,113]. Indeed, we observed significant changes in a number of EV miRNAs in response to CIE vapor treatment (unpublished observations). Additionally, EVs are packaged with DNA, lipids, and proteins, all of which have the potential to alter cellular function[5,7,12]. Beyond the alteration to biological processes, characterizing these changes may also allow for the identification of circulating biomarkers for AUD. In fact, recent studies have already begun this work, with a novel circRNA being identified in serum EVs and correlating strongly with alcohol dependence[114]. Future studies should expand upon what we have begun here and investigate changes in EV content of other biomolecules.

It is important to emphasize that EVs in this study were isolated from whole brain tissue, which has the possibility to mask cell-type or brain region specific changes that may be occurring. Additionally, EVs have the ability to cross the blood-brain-barrier[115–117], so these EVs may have originated outside of the CNS. We know from previous studies that the microRNA content of liver EVs is altered following alcohol exposure[29–31]. Introduction of these EVs to ethanol naïve monocytes sensitizes the monocytes response to LPS[28], demonstrating the ability of EV cargo to change functional outcomes of recipient cells. As discussed above, isolation of EVs from primary cell culture has already indicated that the proinflammatory content of microglial and astrocyte EVs increases following ethanol[17,18]. We observed a slight change in neuroinflammatory gene expression in our results, but the findings may have been more robust had we been able to determine the cell of origin for each EV. While the technology is still in its infancy, methods to determine tissue and cell type of origin from heterogeneous EV populations are being developed and will help researchers understand cell-specific contributions to EV populations and how various cell-types change EV packaging and release in response to perturbation[118,119].

There are a few limitations of our study. First, the two CIE vapor treatments used in these experiments are somewhat different. In addition to differing amounts of time spent in the CIE vapor chambers, animals used as EV donors for electrophysiology

experiments were pretreated with pyrazole +/- ethanol. We acknowledge that the two treatment paradigms may produce distinct changes in CIE EV content and future experiments should investigate how different ethanol exposures, as well as pyrazole treatment, impact brain-derived EVs. Second, while we characterized our EVs using NTA and EM and demonstrated the vesicles were of the expected size range and shape, we did not determine which surface proteins these EVs expressed. It is possible that vesicles from other organelles, such as Golgi, could co-purify with our EVs. Studies employing a similar ultracentrifuge method, though, have shown that EVs collected through this protocol do display classic EV protein markers[55,120–122]. Additionally, we did not test non-EV containing supernatant in our electrophysiology experiments. Future experiments would include this control to determine if a remaining soluble component in the supernatant has the ability to impact cell firing. Finally, as part of these experiments, we did not independently verify that EVs were taken up by the D1 neurons.

The experiments described here only begin to uncover how ethanol impacts EV processing and how these EVs impact neuronal function *ex vivo*. An interesting line of research to pursue in the future would be studying the effects of ethanol-primed EVs *in vivo*. Many studies have demonstrated the feasibility of treating live rodents with EVs, either through intracerebroventricular or intranasal administration, and that this treatment has the ability to significantly alter behavior[123–128]. Some studies highlight the ability of EVs to induce pathology in healthy animals, such as an increase in depressive-like behavior in rodents who received EVs from patients with major depressive disorder[126]. This is not always the case, as many studies also underscore the potential benefits of EV administration, with attenuation of behaviors associated with autism[128], Parkinson's[124], and traumatic brain injury[125,127] observed following treatment. One study by Ezquer et al. demonstrated that intranasal administration of mesenchymal stem cell-derived EVs reduced ethanol consumption and oxidative stress in chronically drinking animals[123]. Understanding how treatment with ethanol primed EVs may impact functional outcomes such as behavior, as well as unraveling the mechanisms by which EVs may be used as a therapeutic for AUD, would greatly enhance our knowledge of the disorder.

Our results indicate that CIE vapor exposure significantly alters EV content in a manner that contributes to many of the negative consequences associated with AUD, such as increases in neuroinflammation, changes in synaptic transmission, and cell death. Results from this and future studies will contribute to our knowledge regarding the perpetuation of AUD and associated consequences, such as synaptic organizational changes and may lead to us to uncover new therapeutic targets for the treatment of this disorder.

**Supplementary Materials:** The following are available, **Figure S1**: Nanoparticle tracking analysis of brain-derived extracellular vesicles from treatment group 2, **Figure S2:** Supplemental electrophysiological results, **Table S1**: All probes detected in total RNA isolated from female brain-derived extracellular vesicles, **Table S2**: Enrichr results for differentially expressed probe targets from female brain-derived extracellular vesicles, **Table S3**: All probes detected in total RNA isolated from male brain-derived extracellular vesicles, **Table S4**: Enrichr results for differentially expressed probe targets from male brain-derived extracellular vesicles, **Table S5**: Significantly differentially expressed probes in common between male and female brain-derived extracellular vesicle, **Table S6**: Weighted gene co-expression network analysis of total RNA isolated from female brain-derived extracellular vesicles, and **Table S7**: Weighted gene co-expression network analysis of total RNA isolated from male brain-derived extracellular vesicles.

**Author Contributions:** Conceptualization, A.B. and G.H.; methodology, A.B., R.M., H.A., and M.L.; formal analysis, A.B., R.M., and S.F.; writing—original draft preparation, A.B and R.M.; writing—review

and editing, A.B., R.M., S.F., M.L., and G.H. All authors have read and agreed to the published version of the manuscript.

**Funding:** This work was funded by NIH/NIAAA grants AA029942 (Baratta), AA020889 (Homanics), AA10422 (Homanics), T32 NS007433-22 (Sved), AA020929 (Lopez), AA024836 (Farris), AA016651 (Mangieri) and 1S10RR019003-01 (Watkins).

**Acknowledgments:** The authors would like to thank the Center for Biologic Imaging at the University of Pittsburgh and the Nanomedicines Characterization Core Facility (NCore) at the University of North Carolina, Chapel Hill for their assistance with this study.

**Conflicts of Interest:** Authors have no conflicts of interest.

**Data Availability Statement:** All microarray expression data has been uploaded to the NIH Gene Expression Omnibus and can be found with accession number GSE194161.

**References**


1. Centers for Disease Control and Prevention (CDC). Alcohol and Public Health: Alcohol-Related Disease Impact (ARDI). AnnualAverage for United States 2011–2015 Alcohol-Attributable Deaths Due toExcessive Alcohol Use, All Ages. . *https://nccd.cdc.gov/DPH_ARDI/Default/Default.aspx.* (2020).

2. Volkow, N. D. & Boyle, M. Neuroscience of addiction: relevance to prevention and treatment. *Am. J. Psychiatry* **175**, 729–740 (2018).

3. Feng, D. *et al.* Cellular internalization of exosomes occurs through phagocytosis. *Traffic* **11**, 675–687 (2010).

4. Morelli, A. E. *et al.* Endocytosis, intracellular sorting, and processing of exosomes by dendritic cells. *Blood* **104**, 3257–3266 (2004).

5. Llorente, A. *et al.* Molecular lipidomics of exosomes released by PC-3 prostate cancer cells. *Biochim. Biophys. Acta* **1831**, 1302–1309 (2013).

6. Laulagnier, K. *et al.* Mast cell- and dendritic cell-derived exosomes display a specific lipid composition and an unusual membrane organization. *Biochem. J.* **380**, 161–171 (2004).

7. Théry, C. *et al.* Proteomic analysis of dendritic cell-derived exosomes: a secreted subcellular compartment distinct from apoptotic vesicles. *J. Immunol.* **166**, 7309–7318 (2001).

8. Mathivanan, S., Fahner, C. J., Reid, G. E. & Simpson, R. J. ExoCarta 2012: database of exosomal proteins, RNA and lipids. *Nucleic Acids Res.* **40**, D1241-4 (2012).

9. Valadi, H. *et al.* Exosome-mediated transfer of mRNAs and microRNAs is a novel mechanism of genetic exchange between cells. *Nat. Cell Biol.* **9**, 654–659 (2007).

10. Montecalvo, A. *et al.* Mechanism of transfer of functional microRNAs between mouse dendritic cells via exosomes. *Blood* **119**, 756–766 (2012).

11. Nolte-'t Hoen, E. N. M. *et al.* Deep sequencing of RNA from immune cell-derived vesicles uncovers the selective incorporation of small non-coding RNA biotypes with potential regulatory functions. *Nucleic Acids Res.* **40**, 9272–9285 (2012).

12. Kim, K. M., Abdelmohsen, K., Mustapic, M., Kapogiannis, D. & Gorospe, M. RNA in extracellular vesicles. *Wiley Interdiscip. Rev. RNA* **8**, (2017).

13. Yoon, Y. J., Kim, O. Y. & Gho, Y. S. Extracellular vesicles as emerging intercellular communicasomes. *BMB Rep.* **47**, 531–539 (2014).

14. Lukiw, W. J. & Pogue, A. I. Vesicular Transport of Encapsulated microRNA between Glial and Neuronal Cells. *Int. J. Mol. Sci.* **21**, (2020).

15. Sharma, P. *et al.* Exosomes regulate neurogenesis and circuit assembly. *Proc Natl Acad Sci USA* **116**, 16086–16094 (2019).

16. Men, Y. *et al.* Exosome reporter mice reveal the involvement of exosomes in mediating neuron to astroglia communication in the CNS. *Nat. Commun.* **10**, 4136 (2019).

17. Pascual, M., Ibáñez, F. & Guerri, C. Exosomes as mediators of neuron-glia communication in neuroinflammation. *Neural Regen. Res.* **15**, 796–801 (2020).

18. Crews, F. T., Zou, J. & Coleman, L. G. Extracellular microvesicles promote microglia-mediated pro-inflammatory responses to ethanol. *J. Neurosci. Res.* (2021) doi:10.1002/jnr.24813.

19. Ma, J. *et al.* Chronic-plus-binge alcohol intake induces production of proinflammatory mtDNA-enriched extracellular vesicles and steatohepatitis via ASK1/p38MAPKα-dependent mechanisms. *JCI Insight* **5**, (2020).

20. Marostica, G., Gelibter, S., Gironi, M., Nigro, A. & Furlan, R. Extracellular vesicles in neuroinflammation. *Front. Cell Dev. Biol.* **8**, 623039 (2020).

21. Saman, S. *et al.* Exosome-associated tau is secreted in tauopathy models and is selectively phosphorylated in cerebrospinal fluid in early Alzheimer disease. *J. Biol. Chem.* **287**, 3842–3849 (2012).

22. Takahashi, R. H. *et al.* Intraneuronal Alzheimer abeta42 accumulates in multivesicular bodies and is associated with synaptic pathology. *Am. J. Pathol.* **161**, 1869–1879 (2002).

23. Verbeek, M. M., Otte-Höller, I., Fransen, J. A. M. & de Waal, R. M. W. Accumulation of the amyloid-beta precursor protein in multivesicular body-like organelles. *J. Histochem. Cytochem.* **50**, 681–690 (2002).

24. Song, Z. *et al.* Brain Derived Exosomes Are a Double-Edged Sword in Alzheimer's Disease. *Front. Mol. Neurosci.* **13**, 79 (2020).

25. Harrison, E. B. *et al.* Traumatic brain injury increases levels of miR-21 in extracellular vesicles: implications for neuroinflammation. *FEBS Open Bio* **6**, 835–846 (2016).

26. Zhao, C. *et al.* Decreased Level of Exosomal miR-5121 Released from Microglia Suppresses Neurite Outgrowth and Synapse Recovery of Neurons Following Traumatic Brain Injury. *Neurotherapeutics* **18**, 1273–1294 (2021).

27. Nielsen, M. C., Andersen, M. N., Grønbæk, H., Damgaard Sandahl, T. & Møller, H. J. Extracellular vesicle-associated soluble CD163 and CD206 in patients with acute and chronic inflammatory liver disease. *Scand. J. Gastroenterol.* **55**, 588–596 (2020).

28. Momen-Heravi, F., Bala, S., Kodys, K. & Szabo, G. Exosomes derived from alcohol-treated hepatocytes horizontally transfer liver specific miRNA-122 and sensitize monocytes to LPS. *Sci. Rep.* **5**, 9991 (2015).

29. Bala, S. *et al.* Circulating microRNAs in exosomes indicate hepatocyte injury and inflammation in alcoholic, drug-induced, and inflammatory liver diseases. *Hepatology* **56**, 1946–1957 (2012).

30. Momen-Heravi, F. *et al.* Increased number of circulating exosomes and their microRNA cargos are potential novel biomarkers in alcoholic hepatitis. *J. Transl. Med.* **13**, 261 (2015).

31. Momen-Heravi, F., Bala, S., Bukong, T. & Szabo, G. Exosome-mediated delivery of functionally active miRNA-155 inhibitor to macrophages. *Nanomedicine* **10**, 1517–1527 (2014).

32. Coleman, L. G., Zou, J. & Crews, F. T. Microglial-derived miRNA let-7 and HMGB1 contribute to ethanol-induced neurotoxicity via TLR7. *J. Neuroinflammation* **14**, 22 (2017).

33. Ibáñez, F., Montesinos, J., Ureña-Peralta, J. R., Guerri, C. & Pascual, M. TLR4 participates in the transmission of ethanol-induced neuroinflammation via astrocyte-derived extracellular vesicles. *J. Neuroinflammation* **16**, 136 (2019).

34. Crenshaw, B. J. *et al.* Alcohol Modulates the Biogenesis and Composition of Microglia-Derived Exosomes. *Biology (Basel)* **8**, (2019).

35. Peng, H., Harvey, B. T., Richards, C. I. & Nixon, K. Neuron-Derived Extracellular Vesicles Modulate Microglia Activation and Function. *Biology (Basel)* **10**, (2021).

36. Sun, Q., Hao, Q. & Prasanth, K. V. Nuclear long noncoding rnas: key regulators of gene expression. *Trends Genet.* **34**, 142–157 (2018).

37. Long, Y., Wang, X., Youmans, D. T. & Cech, T. R. How do lncRNAs regulate transcription? *Sci. Adv.* **3**, eaao2110 (2017).

38. Teng, L. *et al.* The pan-cancer lncRNA PLANE regulates an alternative splicing program to promote cancer pathogenesis. *Nat. Commun.* **12**, 3734 (2021).

39. Lan, Z. *et al.* The Interaction Between lncRNA SNHG6 and hnRNPA1 Contributes to the Growth of Colorectal Cancer by Enhancing Aerobic Glycolysis Through the Regulation of Alternative Splicing of PKM. *Front. Oncol.* **10**, 363 (2020).

40. Chang, L., Guo, R., Yuan, Z., Shi, H. & Zhang, D. LncRNA HOTAIR Regulates CCND1 and CCND2 Expression by Sponging miR-206 in Ovarian Cancer. *Cell. Physiol. Biochem.* **49**, 1289–1303 (2018).

41. Huang, J.-K. *et al.* LncRNA-MALAT1 Promotes Angiogenesis of Thyroid Cancer by Modulating Tumor-Associated Macrophage FGF2 Protein Secretion. *J. Cell. Biochem.* **118**, 4821–4830 (2017).

42. Patel, N. A. *et al.* Long noncoding RNA MALAT1 in exosomes drives regenerative function and modulates inflammation-linked networks following traumatic brain injury. *J. Neuroinflammation* **15**, 204 (2018).

43. Dragomir, M., Chen, B. & Calin, G. A. Exosomal lncRNAs as new players in cell-to-cell communication. *Transl. Cancer Res.* **7**, S243–S252 (2018).

44. Saba, L. M. *et al.* A long non-coding RNA (Lrap) modulates brain gene expression and levels of alcohol consumption in rats. *Genes Brain Behav.* **20**, e12698 (2021).

45. Bohnsack, J. P., Teppen, T., Kyzar, E. J., Dzitoyeva, S. & Pandey, S. C. The lncRNA BDNF-AS is an epigenetic regulator in the human amygdala in early onset alcohol use disorders. *Transl. Psychiatry* **9**, 34 (2019).

46. Griffin, W. C., Haun, H. L., Hazelbaker, C. L., Ramachandra, V. S. & Becker, H. C. Increased extracellular glutamate in the nucleus accumbens promotes excessive ethanol drinking in ethanol dependent mice. *Neuropsychopharmacology* **39**, 707–717 (2014).

47. Rassnick, S., Pulvirenti, L. & Koob, G. F. Oral ethanol self-administration in rats is reduced by the administration of dopamine and glutamate receptor antagonists into the nucleus accumbens. *Psychopharmacology (Berl)* **109**, 92–98 (1992).

48. Moghaddam, B. & Bolinao, M. L. Biphasic effect of ethanol on extracellular accumulation of glutamate in the hippocampus and the nucleus accumbens. *Neurosci. Lett.* **178**, 99–102 (1994).

49. Rathod, R. S. *et al.* Effects of paternal preconception vapor alcohol exposure paradigms on behavioral responses in offspring. *Brain Sci.* **10**, (2020).

50. Rompala, G. R., Finegersh, A., Slater, M. & Homanics, G. E. Paternal preconception alcohol exposure imparts intergenerational alcohol-related behaviors to male offspring on a pure C57BL/6J background. *Alcohol* **60**, 169–177 (2017).

51. Rompala, G. R., Finegersh, A. & Homanics, G. E. Paternal preconception ethanol exposure blunts hypothalamic-pituitary-adrenal axis responsivity and stress-induced excessive fluid intake in male mice. *Alcohol* **53**, 19–25 (2016).

52. Finegersh, A. & Homanics, G. E. Paternal alcohol exposure reduces alcohol drinking and increases behavioral sensitivity to alcohol selectively in male offspring. *PLoS ONE* **9**, e99078 (2014).

53. Becker, H. C. & Lopez, M. F. Increased ethanol drinking after repeated chronic ethanol exposure and withdrawal experience in C57BL/6 mice. *Alcohol. Clin. Exp. Res.* **28**, 1829–1838 (2004).

54. Lopez, M. F. & Becker, H. C. Effect of pattern and number of chronic ethanol exposures on subsequent voluntary ethanol intake in C57BL/6J mice. *Psychopharmacology (Berl)* **181**, 688–696 (2005).

55. Pérez-González, R. *et al.* A Method for Isolation of Extracellular Vesicles and Characterization of Exosomes from Brain Extracellular Space. *Methods Mol. Biol.* **1545**, 139–151 (2017).

56. Łabaj, P. P. *et al.* Characterization and improvement of RNA-Seq precision in quantitative transcript expression profiling. *Bioinformatics* **27**, i383-91 (2011).

57. Chen, E. Y. *et al.* Enrichr: interactive and collaborative HTML5 gene list enrichment analysis tool. *BMC Bioinformatics* **14**, 128 (2013).

58. Kuleshov, M. V. *et al.* Enrichr: a comprehensive gene set enrichment analysis web server 2016 update. *Nucleic Acids Res.* **44**, W90-7 (2016).

59. Langfelder, P. & Horvath, S. WGCNA: an R package for weighted correlation network analysis. *BMC Bioinformatics* **9**, 559 (2008).

60. Ade, K. K., Wan, Y., Chen, M., Gloss, B. & Calakos, N. An improved BAC transgenic fluorescent reporter line for sensitive and specific identification of striatonigral medium spiny neurons. *Front. Syst. Neurosci.* **5**, 32 (2011).

61. Lieberman, O. J. *et al.* Cell-type-specific regulation of neuronal intrinsic excitability by macroautophagy. *eLife* **9**, (2020).

62. Renteria, R., Maier, E. Y., Buske, T. R. & Morrisett, R. A. Selective alterations of NMDAR function and plasticity in D1 and D2 medium spiny neurons in the nucleus accumbens shell following chronic intermittent ethanol exposure. *Neuropharmacology* **112**, 164–171 (2017).

63. Kircher, D. M., Aziz, H. C., Mangieri, R. A. & Morrisett, R. A. Ethanol Experience Enhances Glutamatergic Ventral Hippocampal Inputs to D1 Receptor-Expressing

Medium Spiny Neurons in the Nucleus Accumbens Shell. *J. Neurosci.* **39**, 2459–2469 (2019).

64. Hwa, L. S. *et al.* Predator odor increases avoidance and glutamatergic synaptic transmission in the prelimbic cortex via corticotropin-releasing factor receptor 1 signaling. *Neuropsychopharmacology* **44**, 766–775 (2019).

65. Mathivanan, S., Ji, H. & Simpson, R. J. Exosomes: extracellular organelles important in intercellular communication. *J. Proteomics* **73**, 1907–1920 (2010).

66. Atay, S., Gercel-Taylor, C., Kesimer, M. & Taylor, D. D. Morphologic and proteomic characterization of exosomes released by cultured extravillous trophoblast cells. *Exp. Cell Res.* **317**, 1192–1202 (2011).

67. Even-Chen, O. & Barak, S. Inhibition of FGF Receptor-1 Suppresses Alcohol Consumption: Role of PI3 Kinase Signaling in Dorsomedial Striatum. *J. Neurosci.* **39**, 7947–7957 (2019).

68. Young, C. *et al.* Ethanol-induced neuronal apoptosis in vivo requires BAX in the developing mouse brain. *Cell Death Differ.* **10**, 1148–1155 (2003).

69. Zhou, Z., Sun, X. & Kang, Y. J. Ethanol-induced apoptosis in mouse liver: Fas- and cytochrome c-mediated caspase-3 activation pathway. *Am. J. Pathol.* **159**, 329–338 (2001).

70. Light, K. E., Belcher, S. M. & Pierce, D. R. Time course and manner of Purkinje neuron death following a single ethanol exposure on postnatal day 4 in the developing rat. *Neuroscience* **114**, 327–337 (2002).

71. Laguesse, S., Morisot, N., Phamluong, K. & Ron, D. Region specific activation of the AKT and mTORC1 pathway in response to excessive alcohol intake in rodents. *Addict. Biol.* **22**, 1856–1869 (2017).

72. Bell, R. L. *et al.* Gene expression changes in the nucleus accumbens of alcohol-preferring rats following chronic ethanol consumption. *Pharmacol. Biochem. Behav.* **94**, 131–147 (2009).

73. Koken, T., Gursoy, F. & Kahraman, A. Long-term alcohol consumption increases pro-matrix metalloproteinase-9 levels via oxidative stress. *J. Med. Toxicol.* **6**, 126–130 (2010).

74. Yin, L.-T. *et al.* Matrix Metalloproteinase-9 Overexpression Regulates Hippocampal Synaptic Plasticity and Decreases Alcohol Consumption and Preference in Mice. *Neurochem. Res.* **45**, 1902–1912 (2020).

75. Harper, C. The neuropathology of alcohol-related brain damage. *Alcohol Alcohol.* **44**, 136–140 (2009).

76. Skuja, S. *et al.* Protective reactivity and alteration of the brain tissue in alcoholics evidenced by SOD1, MMP9 immunohistochemistry, and electron microscopy. *Ultrastruct. Pathol.* **37**, 346–355 (2013).

77. Tavares, E. R., Silva-Gotay, A., Riad, W. V., Bengston, L. & Richardson, H. N. Sex differences in the effect of alcohol drinking on myelinated axons in the anterior cingulate cortex of adolescent rats. *Brain Sci.* **9**, (2019).

78. Montesinos, J. *et al.* TLR4 elimination prevents synaptic and myelin alterations and long-term cognitive dysfunctions in adolescent mice with intermittent ethanol treatment. *Brain Behav. Immun.* **45**, 233–244 (2015).

79. Daston, M. M. *et al.* The protein product of the neurofibromatosis type 1 gene is expressed at highest abundance in neurons, Schwann cells, and oligodendrocytes. *Neuron* **8**, 415–428 (1992).

80. Nielsen, J. A., Berndt, J. A., Hudson, L. D. & Armstrong, R. C. Myelin transcription factor 1 (Myt1) modulates the proliferation and differentiation of oligodendrocyte lineage cells. *Mol. Cell. Neurosci.* **25**, 111–123 (2004).

81. Balakrishnan, A. *et al.* Insights into the role and potential of schwann cells for peripheral nerve repair from studies of development and injury. *Front. Mol. Neurosci.* **13**, 608442 (2020).

82. Repunte-Canonigo, V. *et al.* Nf1 regulates alcohol dependence-associated excessive drinking and gamma-aminobutyric acid release in the central amygdala in mice and is associated with alcohol dependence in humans. *Biol. Psychiatry* **77**, 870–879 (2015).

83. Bahi, A. & Dreyer, J.-L. Viral-mediated overexpression of the Myelin Transcription Factor 1 (MyT1) in the dentate gyrus attenuates anxiety- and ethanol-related behaviors in rats. *Psychopharmacology (Berl)* **234**, 1829–1840 (2017).

84. Love, S. Demyelinating diseases. *J. Clin. Pathol.* **59**, 1151–1159 (2006).

85. Galazka, G., Mycko, M. P., Selmaj, I., Raine, C. S. & Selmaj, K. W. Multiple sclerosis: Serum-derived exosomes express myelin proteins. *Mult. Scler.* **24**, 449–458 (2018).

86. Lee, J. *et al.* Exosomal proteome analysis of cerebrospinal fluid detects biosignatures of neuromyelitis optica and multiple sclerosis. *Clin. Chim. Acta* **462**, 118–126 (2016).

87. Krämer-Albers, E.-M. *et al.* Oligodendrocytes secrete exosomes containing major myelin and stress-protective proteins: Trophic support for axons? *Proteomics Clin. Appl.* **1**, 1446–1461 (2007).

88. Domingues, H. S., Falcão, A. M., Mendes-Pinto, I., Salgado, A. J. & Teixeira, F. G. Exosome circuitry during (de)(re)myelination of the central nervous system. *Front. Cell Dev. Biol.* **8**, 483 (2020).

89. Bakhti, M., Winter, C. & Simons, M. Inhibition of myelin membrane sheath formation by oligodendrocyte-derived exosome-like vesicles. *J. Biol. Chem.* **286**, 787–796 (2011).

90. Shen, T. *et al.* Pancreatic cancer-derived exosomes induce apoptosis of T lymphocytes through the p38 MAPK-mediated endoplasmic reticulum stress. *FASEB J.* **34**, 8442–8458 (2020).

91. Gambim, M. H. *et al.* Platelet-derived exosomes induce endothelial cell apoptosis through peroxynitrite generation: experimental evidence for a novel mechanism of septic vascular dysfunction. *Crit. Care* **11**, R107 (2007).

92. Lin, H. *et al.* Brain-derived extracellular vesicles mediated coagulopathy, inflammation and apoptosis after sepsis. *Thromb. Res.* **207**, 85–95 (2021).

93. Buntinx, M. *et al.* Cytokine-induced cell death in human oligodendroglial cell lines: I. Synergistic effects of IFN-gamma and TNF-alpha on apoptosis. *J. Neurosci. Res.* **76**, 834–845 (2004).

94. Talley, A. K. *et al.* Tumor necrosis factor alpha-induced apoptosis in human neuronal cells: protection by the antioxidant N-acetylcysteine and the genes bcl-2 and crmA. *Mol. Cell. Biol.* **15**, 2359–2366 (1995).

95. Lee, Y. B. *et al.* Role of tumor necrosis factor-alpha in neuronal and glial apoptosis after spinal cord injury. *Exp. Neurol.* **166**, 190–195 (2000).

96. Zhang, L., Dong, L.-Y., Li, Y.-J., Hong, Z. & Wei, W.-S. The microRNA miR-181c controls microglia-mediated neuronal apoptosis by suppressing tumor necrosis factor. *J. Neuroinflammation* **9**, 211 (2012).

97. Jurewicz, A. *et al.* Tumour necrosis factor-induced death of adult human oligodendrocytes is mediated by apoptosis inducing factor. *Brain* **128**, 2675–2688 (2005).

98. Traka, M., Podojil, J. R., McCarthy, D. P., Miller, S. D. & Popko, B. Oligodendrocyte death results in immune-mediated CNS demyelination. *Nat. Neurosci.* **19**, 65–74 (2016).

99. Akassoglou, K. *et al.* Oligodendrocyte apoptosis and primary demyelination induced by local TNF/p55TNF receptor signaling in the central nervous system of transgenic mice: models for multiple sclerosis with primary oligodendrogliopathy. *Am. J. Pathol.* **153**, 801–813 (1998).

100. Guo, X. *et al.* Regulation of the severity of neuroinflammation and demyelination by TLR-ASK1-p38 pathway. *EMBO Mol. Med.* **2**, 504–515 (2010).

101. Patel, R. R. *et al.* Synaptic effects of IL-1β and CRF in the central amygdala after protracted alcohol abstinence in male rhesus macaques. *Neuropsychopharmacology* (2021) doi:10.1038/s41386-021-01231-y.

102. Dutta, R. *et al.* Demyelination causes synaptic alterations in hippocampi from multiple sclerosis patients. *Ann. Neurol.* **69**, 445–454 (2011).

103. Ziehn, M. O. *et al.* Therapeutic testosterone administration preserves excitatory synaptic transmission in the hippocampus during autoimmune demyelinating disease. *J. Neurosci.* **32**, 12312–12324 (2012).

104. Marty, V. N. & Spigelman, I. Effects of alcohol on the membrane excitability and synaptic transmission of medium spiny neurons in the nucleus accumbens. *Alcohol* **46**, 317–327 (2012).

105. Laulagnier, K. *et al.* Amyloid precursor protein products concentrate in a subset of exosomes specifically endocytosed by neurons. *Cell. Mol. Life Sci.* **75**, 757–773 (2018).

106. Yue, K.-Y. *et al.* Neurons can upregulate Cav-1 to increase intake of endothelial cells-derived extracellular vesicles that attenuate apoptosis via miR-1290. *Cell Death Dis.* **10**, 869 (2019).

107. Vilcaes, A. A., Chanaday, N. L. & Kavalali, E. T. Interneuronal exchange and functional integration of synaptobrevin via extracellular vesicles. *Neuron* **109**, 971-983.e5 (2021).

108. Suryanarayanan, A. *et al.* Role of interleukin-10 (IL-10) in regulation of GABAergic transmission and acute response to ethanol. *Neuropharmacology* **107**, 181–188 (2016).

109. Patel, R. R. *et al.* IL-10 normalizes aberrant amygdala GABA transmission and reverses anxiety-like behavior and dependence-induced escalation of alcohol intake. *Prog. Neurobiol.* **199**, 101952 (2021).

110. Mikheeva, I. B., Malkov, A. E., Pavlik, L. L., Arkhipov, V. I. & Levin, S. G. Effect of Interleukin-10 on Localization of AMPA Receptors in Synapses during Long-

Term Posttetanic Potentiation in Cultured Hippocampal Slices. *Bull. Exp. Biol. Med.* **167**, 53–56 (2019).

111. Ishikawa, M. *et al.* Homeostatic synapse-driven membrane plasticity in nucleus accumbens neurons. *J. Neurosci.* **29**, 5820–5831 (2009).

112. Yu, C.-Y. & Kuo, H.-C. The emerging roles and functions of circular RNAs and their generation. *J. Biomed. Sci.* **26**, 29 (2019).

113. Catalanotto, C., Cogoni, C. & Zardo, G. Microrna in control of gene expression: an overview of nuclear functions. *Int. J. Mol. Sci.* **17**, (2016).

114. Liu, Y. *et al.* Circular RNA expression alteration identifies a novel circulating biomarker in serum exosomal for detection of alcohol dependence. *Addict. Biol.* e13031 (2021) doi:10.1111/adb.13031.

115. Zhuang, X. *et al.* Treatment of brain inflammatory diseases by delivering exosome encapsulated anti-inflammatory drugs from the nasal region to the brain. *Mol. Ther.* **19**, 1769–1779 (2011).

116. Chen, C. C. *et al.* Elucidation of Exosome Migration across the Blood-Brain Barrier Model In Vitro. *Cell. Mol. Bioeng.* **9**, 509–529 (2016).

117. Gómez-Molina, C. *et al.* Small Extracellular Vesicles in Rat Serum Contain Astrocyte-Derived Protein Biomarkers of Repetitive Stress. *Int. J. Neuropsychopharmacol.* **22**, 232–246 (2019).

118. Li, Y. *et al.* EV-origin: Enumerating the tissue-cellular origin of circulating extracellular vesicles using exLR profile. *Comput. Struct. Biotechnol. J.* **18**, 2851–2859 (2020).

119. Larssen, P. *et al.* Tracing cellular origin of human exosomes using multiplex proximity extension assays. *Mol. Cell. Proteomics* **16**, 502–511 (2017).

120. Peng, K. Y. *et al.* Apolipoprotein E4 genotype compromises brain exosome production. *Brain* **142**, 163–175 (2019).

121. Mo, L.-J. *et al.* Exosome-packaged miR-1246 contributes to bystander DNA damage by targeting LIG4. *Br. J. Cancer* **119**, 492–502 (2018).

122. Gauthier, S. A. *et al.* Enhanced exosome secretion in Down syndrome brain - a protective mechanism to alleviate neuronal endosomal abnormalities. *Acta Neuropathol. Commun.* **5**, 65 (2017).

123. Ezquer, F. *et al.* Intranasal delivery of mesenchymal stem cell-derived exosomes reduces oxidative stress and markedly inhibits ethanol consumption and post-deprivation relapse drinking. *Addict. Biol.* **24**, 994–1007 (2019).

124. Yang, J. *et al.* Exosome-mediated delivery of antisense oligonucleotides targeting α-synuclein ameliorates the pathology in a mouse model of Parkinson's disease. *Neurobiol. Dis.* **148**, 105218 (2021).

125. Chen, Y. *et al.* MSC-derived exosomes promote recovery from traumatic brain injury via microglia/macrophages in rat. *Aging (Albany NY)* **12**, 18274–18296 (2020).

126. Wei, Z.-X. *et al.* Exosomes from patients with major depression cause depressive-like behaviors in mice with involvement of miR-139-5p-regulated neurogenesis. *Neuropsychopharmacology* **45**, 1050–1058 (2020).

127. Moss, L. D. *et al.* Intranasal delivery of exosomes from human adipose derived stem cells at forty-eight hours post injury reduces motor and cognitive impairments following traumatic brain injury. *Neurochem. Int.* **150**, 105173 (2021).

128. Perets, N., Hertz, S., London, M. & Offen, D. Intranasal administration of exosomes derived from mesenchymal stem cells ameliorates autistic-like behaviors of BTBR mice. *Mol. Autism* **9**, 57 (2018).

## Figure Legends

**Figure 1**. Extracellular vesicle (EV) characterization following chronic intermittent ethanol (CIE) vapor exposure. **(A)** Representative Nanoparticle tracking analysis (NTA) trace showing particle size distribution for CIE EVs isolated by differential ultracentrifugation. **(B)** Electron microscopy image of CIE EVs. No significant change in brain-derived EV **(C)** size or **(D)** concentration of diluted (1:1000) EVs following CIE vapor exposure compared to air exposed controls as assessed by NTA. Data are mean ± SEM; N = 6 males per group.

**Figure 2.** Differentially expressed probe targets (DEPTs) from extracellular vesicle RNA in response to chronic intermittent ethanol vapor exposure. Blue represents significantly down-regulated DEPTs and red represents significantly up-regulated DEPTs. Volcano plots represent **(A)** female mRNA (393 downregulated; 800 upregulated), **(B)** female lncRNA (635 downregulated; 1291 upregulated), **(C)** male mRNA (212 downregulated; 109 upregulated), and **(D)** male lncRNA (330 downregulated; 290 upregulated).

**Figure 3.** Venn diagrams comparing male and female differentially expressed probe targets (DEPTs) of EV RNA following chronic intermittent ethanol vapor exposure. Shown here are results for up-regulated (across the top) and down-regulated (across the bottom) mRNA (left) and lncRNA (right) DEPTs. Males are represented in blue and females in pink. P-value represents significant overlap between male and female samples.

**Figure 4.** Effects of EVs on synaptic transmission in the NAc. **(A)** Representative current traces showing spontaneous excitatory postsynaptic currents (sEPSCs) recorded at -55 mV holding potential. **(B)** Cumulative probability distributions of sEPSC amplitudes in 2.5 pA bins. **(C)** Mean sEPSC amplitudes. **(D)** Cumulative probability distributions of sEPSC area (event charge transfer) in 25 pA*ms bins. **(E)** Mean sEPSC areas (event charge transfer). **(F)** Cumulative probability distributions of sEPSC decay times (90%-10%) in 1 ms bins. **(G)** Mean sEPSC decay times (90%-10%). **(H)** Representative current traces showing spontaneous inhibitory postsynaptic currents (sIPSCs) recorded at +10 mV holding potential. **(I)** Cumulative probability distributions of sIPSC rise times (10%-90%) in 0.5 ms bins. **(J)** Mean sIPSC rise times (10%-90%). Inset shows amplitude-normalized, averaged sIPSC traces from one neuron per group overlaid and aligned at baseline. **(K)** Cumulative probability distributions of sIPSC decay times (90%-10%) in 2 ms bins. **(L)** Best-fit curves overlaid on each group's normalized probability distribution (histogram of binned data), with corresponding $R^2$ values for each curve. Inset shows amplitude-normalized, peak-aligned, averaged sIPSC traces for slow and fast-decaying events from one neuron per group. **(M)** Mean sIPSC decay times (90%-10%). Bar graphs show individual data for each neuron (circles) overlaid on group means ± sem (bars). Cumulative probability distributions of binned data show group means ± sem. For all sEPSC data, group n's (neurons/mice) = 13/5, PBS control, 12/5, Air, 11/6, CIE. For sIPSC data shown here, n's (neurons/mice)

= 10/5, PBS control, 10/5, Air, 10/6, CIE. When Air and CIE distributions did not differ from each other they are shown in the panel insets using the same ranges of x- and y-axes as the main panel, and the cumulative distributions of the pooled data from these two groups are shown by the “EVs” plots in the main panels. Dashed lines are used to indicate significance for 2-way ANOVAs comparing all three groups; solid lines are used to indicate significance between two groups. *, ****, P < 0.05, 0.0001, effect of group in t-test, Tukey’s multiple comparisons, F-test, or 2-way ANOVA. ##, ###, ####, P < 0.01, 0.001, 0.0001, bin x group interaction in two-way ANOVA. †, p <0.05, CIE vs. PBS for the indicated bin, Tukey’s multiple comparisons.

**Table 1.** Top 10 differentially expressed probe targets in female brain-derived extracellular vesicle RNA samples following chronic intermittent ethanol vapor exposure compared to air exposed controls.

| Probe Name | P-Value | Fold Change | Gene Symbol | RNA Type |
|---|---|---|---|---|
| ASMM10P046336V4 | 0.00017791 | 2.403 | *AK155383* | lncRNA |
| ASMM10LNC1A107018953V4 | 0.00028268 | 2.495 | *Tcl1* | lncRNA |
| ASMM10AP1B104860564V4 | 0.00047037 | 2.034 | *Ppp2r3a* | Protein coding |
| ASMM10LNC1A100117190V4 | 0.00048895 | 2.704 | *AK149852* | lncRNA |
| ASMM10P025479V4 | 0.00055746 | 2.454 | *AK149827* | lncRNA |
| ASMM10AP1B113124604V4 | 0.00058461 | 2.926 | *Mkrn2* | Protein coding |
| ASMM10AP1B111869791V4 | 0.00061308 | 2.293 | *Slc13a4* | Protein coding |
| ASMM10AP1B100182324V4 | 0.00062297 | 2.291 | *Sall1* | Protein coding |
| ASMM10AP1B100182324V4 | 0.00063632 | 3.114 | *4930588G17Rik* | lncRNA |
| ASMM10LNC1A102689698V4 | 0.00064908 | 2.025 | *Dennd1c* | lncRNA |

**Table 2.** Biological processes differentially regulated in female brain-derived extracellular vesicles.

| ID | Name | # DE/# in category | P-Value |
|---|---|---|---|
| GO:1904749 | regulation of protein localization to nucleolus | 4/8 | 1.59E-04 |
| GO:0086005 | ventricular cardiac muscle cell action potential | 5/18 | 5.74E-04 |
| GO:0032479 | regulation of type I interferon production | 10/89 | 0.00301396 |
| GO:0032467 | positive regulation of cytokinesis | 4/17 | 0.00331605 |
| GO:0010881 | regulation of cardiac muscle contraction by regulation of the release of sequestered calcium ion | 2/17 | 0.00405731 |
| GO:0008016 | regulation of heart contraction | 10/93 | 0.00415098 |
| GO:0006513 | protein monoubiquitination | 6/39 | 0.00434833 |
| GO:0060307 | regulation of ventricular cardiac muscle cell membrane repolarization | 4/18 | 0.00505262 |
| GO:0045216 | cell-cell junction organization | 9/82 | 0.00558606 |
| GO:0086002 | cardiac muscle cell action potential involved in contraction | 5/31 | 0.00738909 |

**Table 3.** Top 10 differentially expressed probe targets in male brain-derived extracellular vesicle RNA samples following chronic intermittent ethanol vapor exposure compared to air exposed controls.

| Probe Name | P-Value | Fold Change | Gene Symbol | RNA Type |
|---|---|---|---|---|
| ASMM10LNC1A100177954V4 | 0.00054982 | 2.053 | *Brd8* | lncRNA |
| ASMM10LNC1A100857462V4 | 0.00118685 | 1.708 | *Casz1* | lncRNA |
| ASMM10AP1B100291592V4 | 0.00164889 | 0.535 | *Sgce* | Protein coding |
| ASMM10P051674V4 | 0.00209351 | 2.366 | *AK087646* | lncRNA |
| ASMM10LNC1A100084059V4 | 0.00216183 | 1.862 | *Hspbp1* | lncRNA |
| ASMM10AP1B121362660V4 | 0.0021792 | 0.561 | *Snx14* | Protein coding |
| ASMM10LNC1A105141278V4 | 0.00299041 | 0.617 | *4933427I22Rik* | lncRNA |
| ASMM10LNC1A106516188V4 | 0.00327777 | 1.712 | *9930038B18Rik* | lncRNA |
| ASMM10LNC1A111657709V4 | 0.00360722 | 1.494 | *9930014A18Rik* | lncRNA |
| ASMM10P050132V4 | 0.00371942 | 0.638 | *AK027997* | lncRNA |

**Table 4.** Biological processes differentially regulated in male brain-derived extracellular vesicles.

| ID | Name | # DE/# in category | P-Value |
|---|---|---|---|
| GO:0005007 | fibroblast growth factor-activated receptor activity | 4/8 | 1.59E-04 |
| GO:0080025 | phosphatidylinositol-3,5-bisphosphate binding | 5/18 | 5.74E-04 |
| GO:0015079 | potassium ion transmembrane transporter activity | 10/89 | 0.00301396 |
| GO:0070697 | activin receptor binding | 4/17 | 0.00331605 |
| GO:0031690 | adrenergic receptor binding | 2/17 | 0.00405731 |
| GO:0046982 | protein heterodimerization activity | 10/93 | 0.00415098 |
| GO:0005267 | potassium channel activity | 6/39 | 0.00434833 |
| GO:0030506 | ankyrin binding | 4/18 | 0.00505262 |
| GO:0008066 | glutamate receptor activity | 9/82 | 0.00558606 |
| GO:1902936 | phosphatidylinositol bisphosphate binding | 5/31 | 0.00738909 |

**Table 5.** Differentially expressed modules in female brain-derived extracellular vesicle RNA following chronic intermittent ethanol exposure as identified by weight gene co-expression network analysis.

| Module Name | P-Value | Size | Change |
|---|---|---|---|
| FM_9 | 7.47E-197 | 1385 | Up-regulated |
| FM_14 | 3.20E-119 | 1018 | Up-regulated |
| FM_7 | 4.01E-118 | 1697 | Up-regulated |
| FM_1 | 8.27E-105 | 12,547 | Down-regulated |
| FM_17 | 2.86E-57 | 770 | Up-regulated |
| FM_13 | 4.45E-55 | 1103 | Up-regulated |
| FM_3 | 3.89E-33 | 2012 | Down-regulated |
| FM_19 | 1.73E-31 | 655 | Down-regulated |
| FM_0 | 1.20E-29 | 1182 | Up-regulated |
| FM_18 | 2.96E-13 | 709 | Up-regulated |
| FM_11 | 5.45E-08 | 1258 | Up-regulated |
| FM_10 | 5.59E-05 | 1321 | Up-regulated |
| FM_8 | 0.04565968 | 1569 | Down-regulated |

**Table 6.** Differentially expressed modules in male brain-derived extracellular vesicle RNA following chronic intermittent ethanol exposure as identified by weight gene co-expression network analysis.

| Module Name | P-Value | Size | Change |
|---|---|---|---|
| MM_28 | 2.75E-135 | 582 | Up-regulated |
| MM_19 | 3.10E-121 | 870 | Down-regulated |
| MM_14 | 1.12E-52 | 1096 | Up-regulated |
| MM_25 | 8.40E-51 | 701 | Down-regulated |
| MM_31 | 2.77E-22 | 489 | Down-regulated |
| MM_2 | 1.21E-21 | 2414 | Up-regulated |
| MM_5 | 5.75E-21 | 1747 | Down-regulated |
| MM_0 | 4.43E-20 | 1464 | Down-regulated |
| MM_33 | 3.95E-06 | 465 | Down-regulated |
| MM_13 | 0.00103725 | 1098 | Up-regulated |
| MM_20 | 0.04121716 | 859 | Up-regulated |

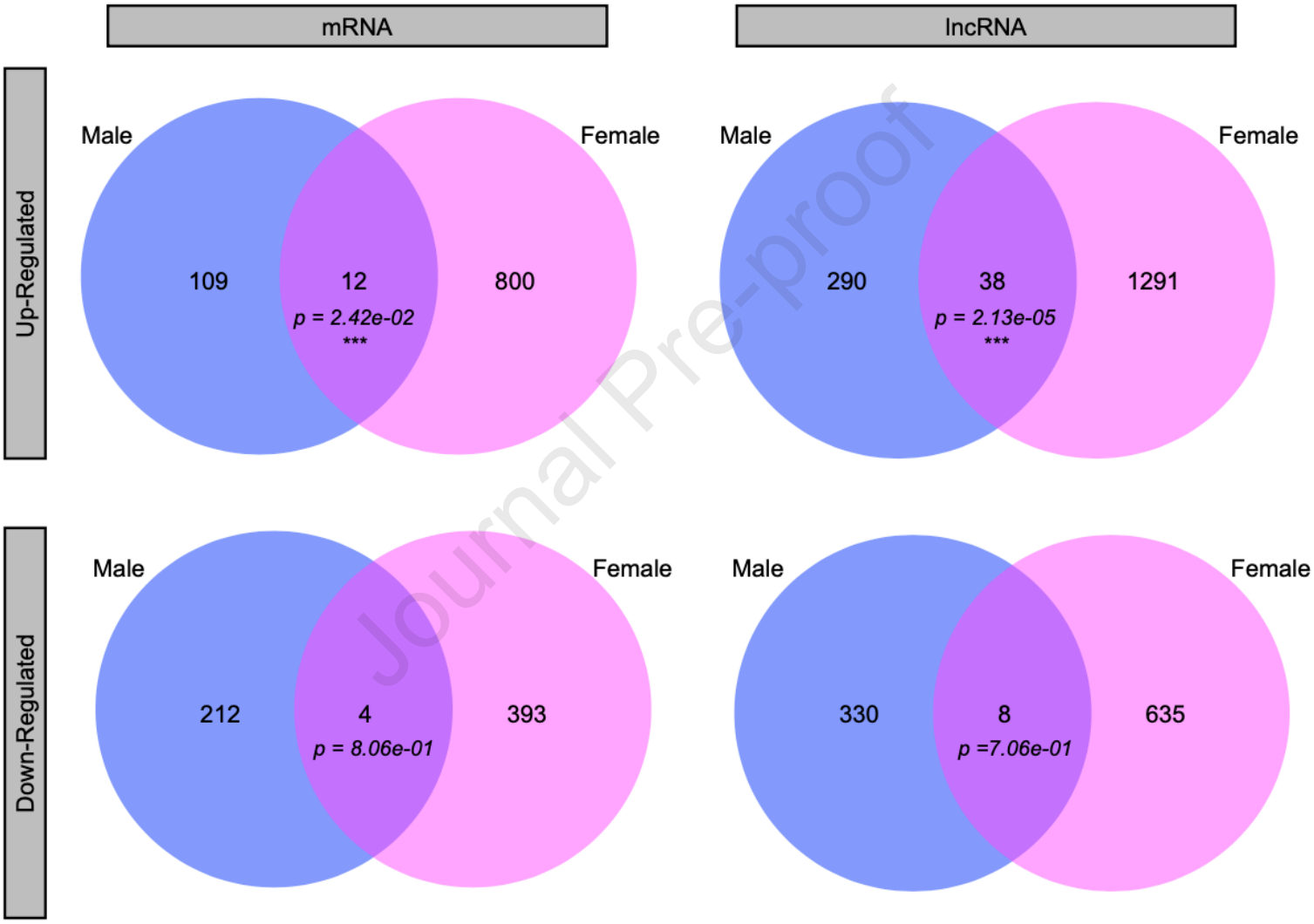

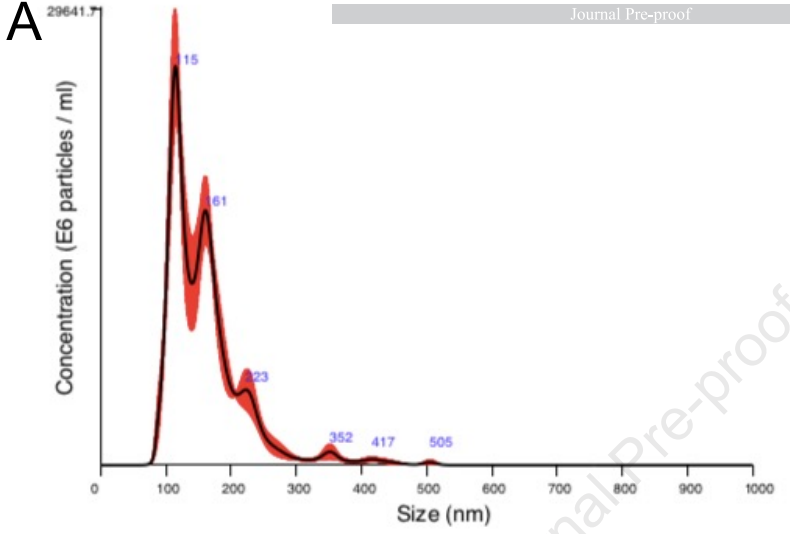


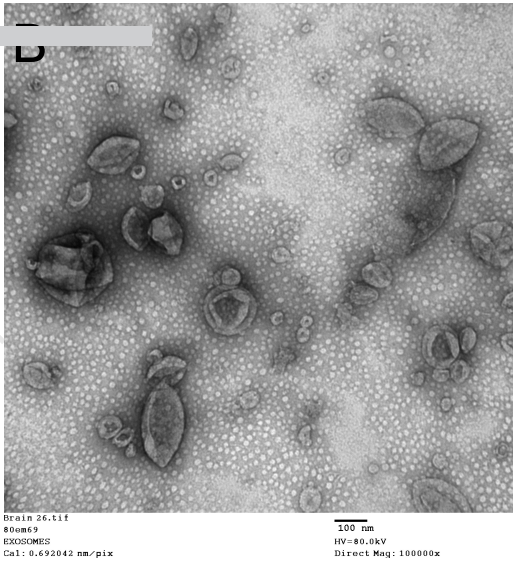


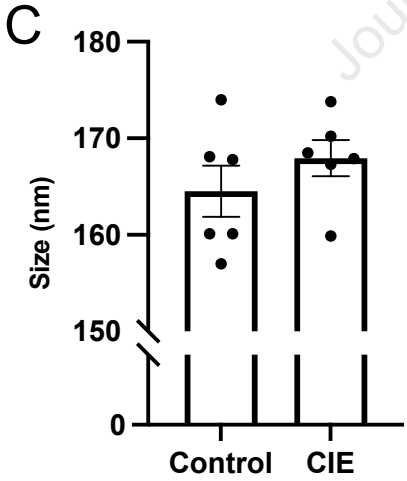


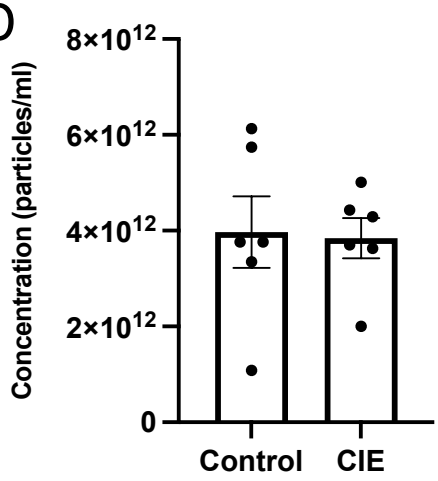

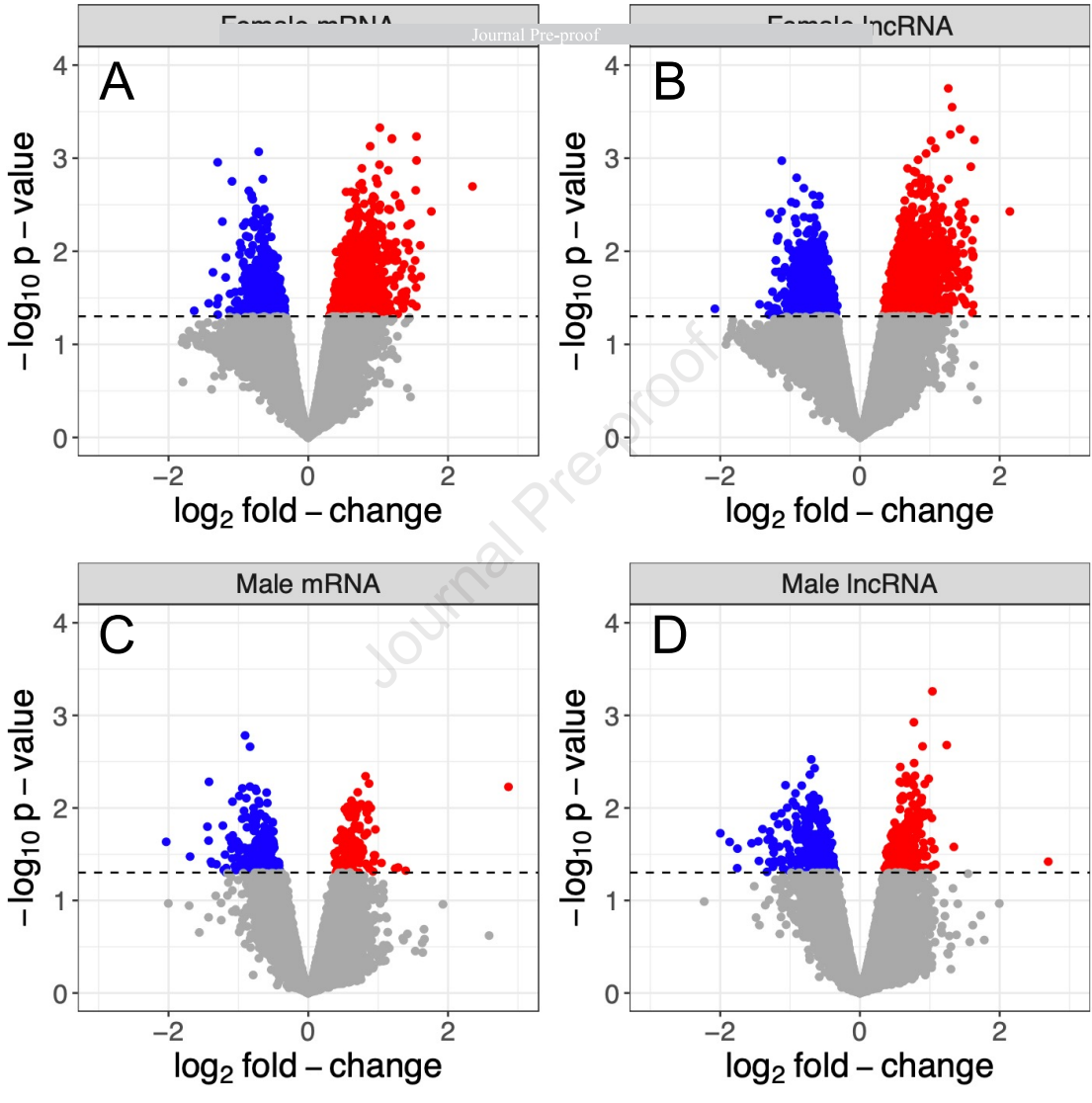

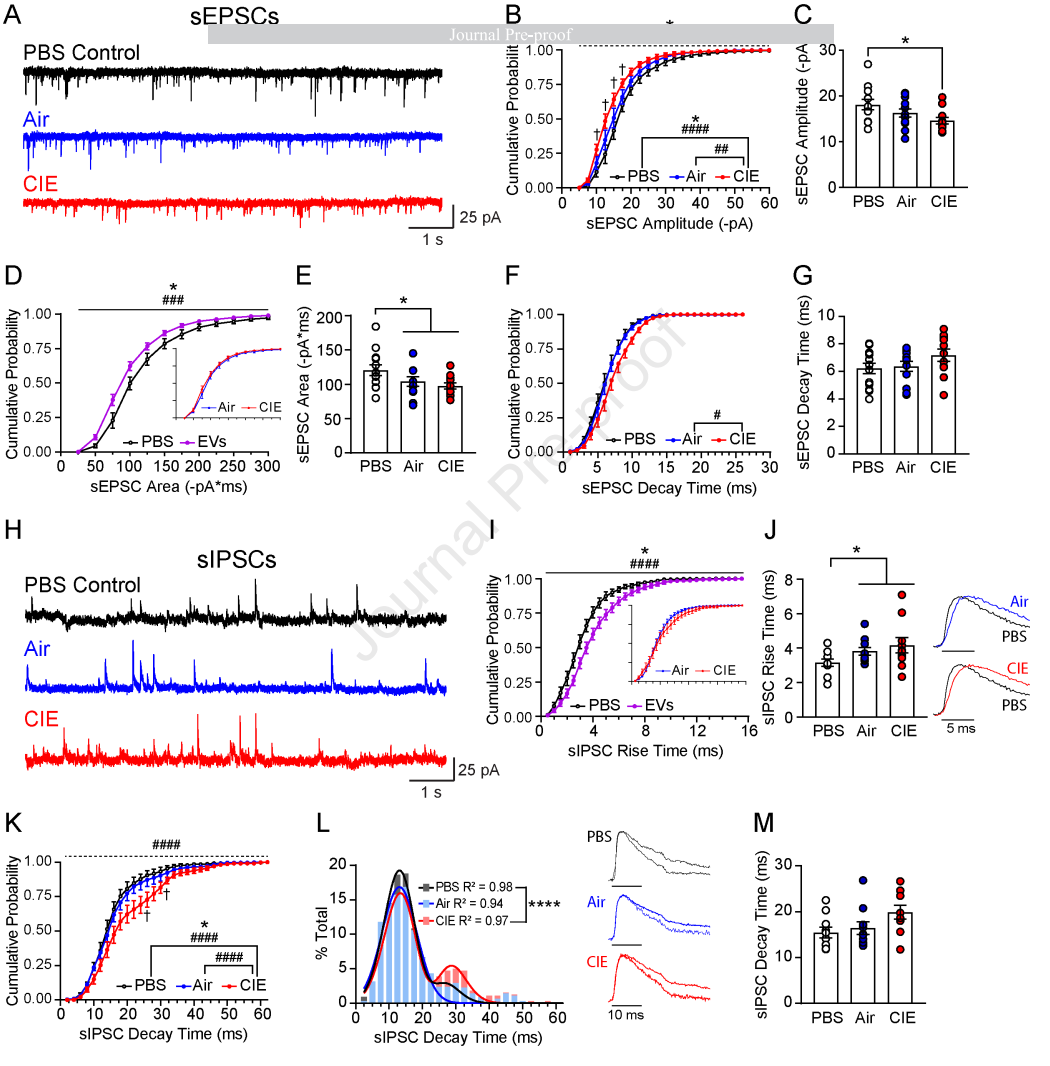

**Highlights:**

- CIE exposure leads to changes in RNA cargo of brain-derived extracellular vesicles
- LncRNA showed greater changes than mRNA following ethanol exposure
- RNA changes were related to neuroinflammation, myelination, and cell death

**Author Contributions:** Conceptualization, A.B. and G.H.; methodology, A.B., R.M., H.A., and M.L.; formal analysis, A.B., R.M., and S.F.; writing—original draft preparation, A.B and R.M.; writing—review and editing, A.B., R.M., S.F., M.L., and G.H. All authors have read and agreed to the published version of the manuscript.